Fabrication of Phosphatidylserine-Containing Asymmetric Giant Unilamellar Vesicles by Hemifusion

A Major Qualifying Project Report Submitted to the Faculty of

WORCESTER POLYTECHNIC INSTITUTE

In partial fulfillment of the requirements for the

Degree of Bachelor of Science in Biochemistry

Date:
April 25, 2024

Written By:
Jake McDonough

Approved By:
Dr. Arne Gericke

Acknowledgements

I would like to thank Dr. Arne Gericke for granting me the opportunity to work in his research group and for his constant support and guidance. I would also like to thank Trevor Paratore for his invaluable mentorship and assistance throughout my time in the research group. I would like to thank Dr. Alonzo Ross and Peter Oni as well for their advice and insights. Additionally, I would like to thank Bella DeCilio and Hannah Ketelhohn, as well as Trevor Paratore again for their preliminary work which has made this thesis possible. I would also like to thank the Scarlata group for allowing me to use their confocal microscope to complete this thesis. Finally, I would like to thank my family for their unwavering support throughout my academic career.

Abstract

Phosphatidylserine (PS) is an important membrane lipid to study due to the vital role it plays in numerous cellular pathways, but doing so is made difficult by the complexities of biological membranes. Studying PS in model membranes can overcome these challenges, though due to most biological membranes being asymmetric (i.e., having a different inner/outer leaflet composition), these models should be so too to ensure accurate simulation. In this study, a method for preparing PS-containing asymmetric giant unilamellar vesicles (aGUVs) was derived. Ca^{2+} or Mg^{2+} was used to induce hemifusion and subsequent total outer leaflet exchange between symmetric GUVs composed of phosphatidylcholine/acceptor fluorophore, and a supported lipid bilayer composed of phosphatidylcholine/PS/donor fluorophore. EDTA was then added to induce fission. The composition of the resulting aGUVs was evaluated by comparing their donor or acceptor fluorophore intensities to that of symmetric GUVs with compositions equal to the theoretical inner or outer leaflet composition of the aGUVs. aGUVs prepared in both low salt buffer (approximately 50 mM NaCl and 30 mM KCl) and high salt buffer (approximately 100 mM NaCl and 80 mM KCl) gave average fluorophore intensities that were around half those of the symmetric GUVs, indicating they were on average the expected composition. Though intensities of individual aGUVs varied significantly. A data filtering method was developed to exclude aGUVs with compositions significantly different than the theoretical, of which 22% passed. These aGUVs could be used in future studies as compositionally consistent, PS-containing asymmetric model membranes.

Table of Contents

List of Figures

List of Tables

1. Introduction

1,2-diacyl-sn-glycero-3-phospho-L-serine (abbreviated phosphatidylserine or PS) is a membrane lipid consisting of a glycerol backbone bonded to two fatty acyl chains and an anionic phosphoserine headgroup. In eukaryotes, PS accounts for around 10 – 15% of the lipids in the plasma membrane (PM) by mole, around 4% in the endoplasmic reticulum (ER) membrane, and around 1% in mitochondrial membranes (*1*). In addition to being non-uniformly distributed throughout the cell, PS is also asymmetrically distributed across the two leaflets of its membranes. For instance, 96% or more of the PS in human PMs is found in the inner leaflet (*2*). This transbilayer asymmetry is important for some of the functions performed by PS, of which there are many. For example, the reduction of this asymmetry in the PM is essential in apoptosis, where early apoptotic cells transport high amounts of PS to their PM's outer leaflet (*3*), which is later recognized by macrophages responsible for clearing the cell's post-apoptosis remnants (*4*). In addition to apoptosis, PS also contributes to a wide range of intracellular pathways. For instance, proteins such as those in the Ras GTPase and protein kinase C families bind PS on the inner leaflet of the PM, which helps recruit them to the membrane, and could be required for them to enter an active state (*1, 5*). These interactions are largely electrostatic, and mediated through PS' negative charge (*1, 5*).

The anionic nature of PS allows it not only to interact with proteins, but also with metal cations. For instance, PS binds Ca^{2+} to form $Ca(PS)_2$ complexes in membranes (*6*). Molecular dynamic simulations suggest that these complexes form via the interaction of Ca^{2+} with the anionic carboxylate group of PS (*7*). In model systems, $Ca(PS)_2$ complexes cluster to form areas enriched in PS lipids, which are a form of membrane domains, meaning regions in a membrane with a differing composition than the surrounding area (*8, 9*). Current studies suggest that most other divalent cations, such as Mg^{2+}, do not induce PS domain formation like what is seen with Ca^{2+} (*8*).

When studying the interactions that PS lipids have with other species (e.g., proteins, metal cations), model membranes are a useful tool. These are membranes, such as vesicles, produced in vitro that are meant to mimic cellular membranes. Model membranes are often the preferred platform for investigating membrane interactions due to cellular membranes being difficult to probe, and often unclear in their exact composition. However, current methods for reliably producing accurate model membranes for the study of PS are limited. Ideally, these membranes contain a consistent, known fraction of PS lipids that are distributed asymmetrically across the two leaflets, just like what is seen in vivo. Some techniques exist to create membranes like this, but they are not without their flaws. One method involves producing symmetric vesicles (i.e., those with the same inner and outer leaflet composition), then using Ca^{2+} to induce the transport of PS from the outer leaflet to the inner (*10*). Though this method creates vesicles with an asymmetric distribution of PS, the fraction of PS in each leaflet varies considerably between vesicles (*10*). Another technique involves creating a surfactant monolayer of lipids at an organic-aqueous interface, then adding new lipids to the monolayer to create a bilayer, which is then

fissioned into vesicles via centrifugation (*11*). This method can produce asymmetric PS vesicles if the correct lipid mixtures are combined, but vesicles produced this way are limited to sizes much smaller than relevant cellular membranes, such as the eukaryotic PM (*11*). This problem makes the resulting membranes less accurate at modeling cellular membranes. A third method involves using cyclodextrins to transfer the outer leaflet lipids of symmetric vesicles with those from donor vesicles, which can be utilized to make asymmetric PS vesicles given proper selection of donor and acceptor vesicles (*12*). However, the cyclodextrins are difficult to separate from the asymmetric vesicles after preparation, resulting in contaminant cyclodextrins being present with the vesicles, which may interfere with experiments. (*13*).

In this study, the hemifusion method introduced by Enoki et al. (*14*) is investigated as a potential new method for producing PS-containing asymmetric model membranes. This method involves using Ca^{2+} to induce fusion between the outer leaflets of symmetric vesicles and the outer leaflet of a supported lipid bilayer (SLB), meaning a planar membrane noncovalently bound to a surface. The hemifusion of these membranes allows the vesicles to exchange their outer leaflet lipids for those in the SLB. Once this exchange has been given time to occur, chelation of the cations via EDTA is used to cause the fissioning of the vesicle back into solution. It is hypothesized that this method can be used to produce asymmetric PS vesicles by inducing the hemifusion between symmetric vesicles and an SLB containing PS. The resulting membranes could in theory be used as accurate model membranes for the study of PS' interactions.

2. Background

2.1 Biological Membranes

The structure of biological membranes is accurately described by the fluid mosaic model published by Singer and Nicholson in 1972 (*15*) and revised in 2013 (*16*). This model states that membranes consist of lipids that arrange into a bilayer, where each lipid is structured as an extended hydrophobic section attached to a hydrophilic head group (*16*). In each of the bilayer's leaflets, lipids arrange side-by-side to align hydrophobic and hydrophilic regions (*16*). At the bilayer's middle plane, the two leaflets meet end-to-end at their hydrophobic faces (*16*). In addition to lipids, the membrane also contains embedded proteins, which present hydrophobic groups in regions where they enter the membrane's interior (*16*). The final components of the membrane are carbohydrates, which are bonded to certain lipid head groups and embedded proteins (*16*). Thus, biological membranes are a "mosaic" of many different molecules arranged into one complex structure. They are also "fluid," which refers to the fact that lipids and proteins in membranes display high rates of lateral mobility, meaning they can move freely throughout the plane of the bilayer (*16*).

Biological membranes are essential for life and serve numerous functions. Firstly, membranes segregate cells from their external environment, which allows them to have a different chemical composition than their surroundings, thereby enabling the chemical processes needed for cellular functioning to occur (*17*). Furthermore, the internal membranes found in many cells compartmentalize their interior into several regions of distinct composition, allowing different processes to occur in each (*17*). In addition to acting as barriers, membranes also serve as a platform for numerous cellular pathways, including signaling pathways. These typically involve a receptor protein in a membrane receiving a stimulus from the environment, causing it to initiate a series of interactions between proteins and other species (e.g., lipids) which eventually elicit a response (*17*). Many of these interactions occur at the membrane, occurring between species that are within the membrane, or through some means bound to it (*17*).

A key feature of biological membranes is the diversity in their constituent lipids. Each class of membrane lipid is structurally distinct and participates in different functions (*18*). For instance, different lipids are recognized by different proteins in cellular pathways (*18*). In eukaryotes, the major classes of membrane lipids are phosphoglycerides, sphingolipids, and sterols (*18*). Phosphoglycerides are composed of a glycerol backbone bonded to two long acyl chains and a phosphate headgroup. Different phosphoglycerides have this phosphate functionalized in different ways. For example, phosphatidylcholine (PC) contains a choline group bonded to the phosphate, while phosphatidylethanolamine (PE) bonds an ethanolamine. Sphingolipids are generally composed of a three carbon backbone bonded to a hydroxyl, an extended aliphatic chain, a long acyl chain attached via an amide, and a carbohydrate or phosphate head group. Like phosphoglycerides, some sphingolipids have their phosphate head group functionalized. These sphingolipids include sphingomyelin (SM), which has a phosphate head group bonding a choline.

Sterols, which include cholesterol, consist of a hydrocarbon fused ring structure bonded to a hydroxyl head group.

Even within the same cell, different membranes have vastly different lipid compositions (*18*). For example, cholesterol in a typical mammalian cell composes 34% of the total lipids by mole in the PM, but only 8% in the ER membrane (*19*). These differences in composition help diversify membranes with respect to their function, where those with different lipid compositions are able to participate in different lipid-dependent pathways.

In addition to different membranes having varied compositions, the two leaflets of a single biological membrane generally differ in lipid composition as well. This phenomenon is referred to as vertical compositional membrane asymmetry (often shortened to vertical asymmetry or just asymmetry), and is known to occur in most eukaryotic membranes, including the PM, Golgi membrane, and endosomal membranes (*20*). For example, a typical animal cell PM has the majority of its PS and PE in the inner leaflet, while almost all of its PC and SM are in the outer leaflet (*21*). Vertical asymmetry in biological membranes is caused firstly by the fact that many membrane lipids are biosynthesized vectorially, meaning they are made in just one leaflet (*22*). For example, SM in the Golgi membrane is synthesized exclusively on the outer leaflet (*23*). By directing lipid synthesis to just one leaflet, a cell is able to enrich that leaflet in said lipid, thus establishing asymmetry. But vectorial synthesis alone is not enough to establish all of the vertical asymmetries found in biological membranes. Doing so also requires the action of flippases and floppases: enzymes capable of transporting specific lipids between leaflets (*20*). These enzymes typically couple the transport to the degradation of ATP, causing the reaction to be irreversible and thereby making the direction of transport singular (*24*). The term “flippase” generally refers to one of these enzymes that transport lipids to the inner leaflet, while “floppase” refers to one that does so to the outer leaflet (*24*). These enzymes can be used by the cell to continuously move specific lipids to just one leaflet of a membrane, which is a process that will eventually reach a steady-state with the natural transverse diffusion of the lipids. Transverse diffusion refers to diffusion between the leaflets of a bilayer, which is generally very slow for membrane lipids (*20*). For instance, in PC vesicles, the half-life for the total exchange of inner and outer leaflet lipids via transverse diffusion is on the order of hours (*25*). Though less polar lipids like cholesterol can move between leaflets much faster (*26*), the vast majority of membrane lipids have slow transverse diffusion like PC (*20*). Therefore, the steady-state amount of a lipid in each membrane leaflet should heavily favor the leaflet a flippase/floppase is moving it to. This relationship allows these enzymes to enrich certain leaflets in specific lipids, and then maintain this asymmetry. By having asymmetric membranes like this, cells are able to diversify the functions of individual leaflets just as is done with different membranes, where leaflets having different profiles of lipids means they can participate in different lipid-dependent pathways.

Related to vertical asymmetry is lateral compositional membrane asymmetry (often shortened to lateral asymmetry), which refers to when a membrane has a different composition in different regions of each leaflet. In this context, these different regions are called membrane domains. Lateral asymmetry is known to exist in at least certain biological membranes. For

example, the PM of an epithelial cell is separated into two large domains: one that faces the interior of the cavity the epithelium is lining, and one that faces the exterior (*27*). These domains differ in protein and lipid composition, where the former is enriched in sphingolipids and the latter is enriched in PC (*28*). This compositional distinction is maintained primarily through tight junctions in the PM which serve as diffusion barriers to block mixing (*29*). The idea of lateral asymmetry was expanded upon by Kai Simons and Elina Ikonen in 1997, who proposed the existence of lipid rafts (*30*). These are nanodomains (i.e., nanometer-scale membrane domains) with a diameter of 10 – 200 nm that are typically composed of cholesterol, sphingolipids, and saturated acyl chain phosphoglycerides (*31*). Characteristic to rafts, these lipids exist in the liquid-ordered phase, which is a more ordered membrane phase than the one lipids normally adopt in biological membranes (the liquid-disordered phase; *32*). In this case, the order comes from the lipids packing more closely together, with their hydrocarbon chains restricted to more extended conformations (*31*). Lipid rafts are known to form spontaneously in model membranes of the correct lipid composition due to their lipids interacting more strongly with each other than the bulk lipids of the membrane (*31*). The existence of raft domains in vivo remains controversial (*32*), though recent experiments suggest they are found in PMs (*33*). In addition to rafts, many other types of nanodomains are known to form in model membranes given the right conditions. For example, certain divalent cations (e.g., Ca^{2+}) can electrostatically interact with the negative charges on the head groups of anionic lipids (e.g., PS) to form clusters (*34*). These clusters function as nanodomains, though in some in vitro experiments, have been shown to grow to micrometer sizes (*34*). Like rafts, the prevalence of these domains in vivo is currently unknown (*34*). Nevertheless, lateral asymmetry is a useful tool for biological membranes, as it allows for the diversification of membrane function throughout a single leaflet. This effect results from the asymmetry making different regions of the leaflet have dissimilar compositions, thereby allowing them to perform different functions. Lateral asymmetry can also serve as a mechanism to bring interacting species (e.g., lipids, proteins) together, where if the species naturally gather in the same domain, it is more likely they will meet each other and be able to interact.

An effect often seen in laterally asymmetric membranes is domain registration, which refers to the locational overlap of a domain in the outer leaflet with one in the inner leaflet (*35, 36*). This effect is mainly studied in cases where the two domains are of the same type (e.g., two lipid rafts; *35, 36*), though heterogeneous combinations are theoretically possible. Registration is believed to be chiefly caused by the hydrocarbon chains of lipids in a domain interacting more strongly with those in the opposing leaflet when there is registration (*36*). The prevalence of domain coupling in vivo remains unknown, though if it does occur, would be a major driving factor for where specific domains are located.

2.2 Phosphatidylserine

As previously mentioned, PS is a phosphoglyceride with a phosphoserine head group (see Figure 1 for structure). PS' acyl chains are typically between 14 and 19 carbons long, with either two

saturated chains, or one saturated chain and a chain with one trans double bond (*37*). The biosynthesis of PS occurs through two different pathways in mammals (*38*). One of these involves the conversion of a PC lipid into a PS by phosphatidylserine synthase 1, an enzyme that swaps the choline on the lipid's head group with a serine (*38*). The second pathway is similar, but uses PE instead of PC and is catalyzed by phosphatidylserine synthase 2, which replaces the lipid's ethanolamine with a serine (*38*). Meanwhile, biodegradation of PS in mammals generally involves the conversion of the lipid back into PE via decarboxylation of its serine into an ethanolamine, which is catalyzed by phosphatidylserine decarboxylase (*38*). This degradation process may also involve the lysis of the PS' acyl chains or head group by phospholipase enzymes (*38*).

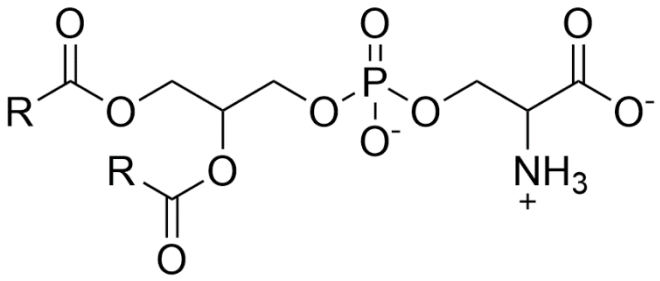

Figure 1. General structure of a PS lipid. R groups are fatty acyl chains, which may be saturated or unsaturated.

In eukaryotes, PS is the most abundant anionic membrane lipid, making up 10% of the cell's total membrane lipid content by mole (*1*). It is distributed unevenly throughout the cell, with around 10 – 15% of lipids in the PM (by mole) being PS, as well as around 4% of those in the ER membrane and around 1% of those in the mitochondrial membranes (*1*). Like most membrane lipids, PS is also distributed unevenly between the leaflets of the membranes it is a part of. For instance, more than 96% of the PS in the human PM is located in the inner leaflet (*2*), while the majority of the PS in the ER membrane is in the inner leaflet (*39*).

PS performs a diverse range of essential functions in cells. Many of these involve the binding of proteins to PS, which is typically mediated through nonspecific electrostatic attractions between a polycationic protein domain and one or more anionic PS head groups (*1*). However, in some cases these interactions are instead mediated through the specific binding of a PS-recognizing protein domain to a PS head group (*5*). In either case, these bindings help recruit the proteins to the membrane and could also help activate them (*38*). The proteins here are generally those involved in cellular pathways (e.g., signaling pathways), and either of these binding effects may be required for the proteins to participate in their pathways. For example, protein kinase C α, a eukaryotic protein kinase utilized in numerous signaling pathways, is recruited to the membrane and driven to its active state by the specific binding of a PS head group to one of its domains (*5*). Without these effects, the kinase would be unable to join the signaling pathways it participates in (*5*).

In addition to interacting with the proteins involved in cellular pathways, PS also participates directly in numerous pathways. For example, as cells start to undergo apoptosis, the outer leaflet of the PM gets progressively enriched in PS by the action of lipid transport enzymes, and the fusion of the PM with lysosomes containing outer leaflet PS (*3, 40*). When the cell eventually breaks off into apoptotic bodies, the exposed PS is recognized by macrophages, allowing them to endocytose the debris (*4*). Therefore, PS enables the clearance of apoptotic bodies following apoptosis.

As was previously explained, PS in membranes (at least, model membranes) is clustered by divalent cations, such as Ca^{2+}, to domains (*8, 9*). In the case of Ca^{2+}, this clustering occurs by the cation binding PS in a 1:2 ratio to form $Ca(PS)_2$ complexes (*6*), with the Ca^{2+} likely associating with both carboxylate charges on the PS (*7*). These $Ca(PS)_2$ complexes then preferentially associate with each other to form domains, which can grow to micrometer sizes in model membranes (*10, 11*). Notably, the lipids in these domains exist in the gel phase, which is a highly ordered membrane phase characterized by the lipids having fully extended, trans chain conformations, and also having very slow lateral diffusion rates (*41*). It is unclear if other divalent cations, like Mg^{2+}, form PS domains in a similar manner to Ca^{2+}. One study fluorescently imaged PS membranes 30 minutes after the introduction of 2 mM Mg^{2+} and saw no domains (*8*), but this could have been due to the domains being too small to resolve. Alternatively, the domains may take longer than 30 minutes to form, which is not unreasonable considering another study found that Ca^{2+}-induced PS domains take around 30 minutes to first form after the introduction of 3 mM Ca^{2+} (*9*).

2.3 Model Membranes

Many interactions at biological membranes, such as those involving PS, are of importance to study. However, doing so in vivo is difficult due to the complexity of biological systems, which makes it difficult to study specific membrane interactions in a controlled manner. For example, in vivo it is challenging to probe these interactions in isolation or do so with precisely known membrane compositions. Therefore, model membranes are often used in place of biological membranes for these studies. These are membranes prepared in vitro that are meant to simulate biological membranes. Many model membranes can be classified as vesicles, meaning enclosed lipid bilayers that contain an aqueous interior (*42*). Other classes of model membranes include planar bilayers, which exist as flat membranes bound to a solid surface (*42*). Overall, there are numerous types of model membranes, each having their own advantages.

SLBs are a specific type of model membrane. These are planar bilayers noncovalently bound to a surface. SLBs can be fabricated through a variety of protocols, such as the vesicle fusion method shown in Figure 2B. In this procedure, small unilamellar vesicles (SUVs) are first prepared (*43*), which are single-bilayer (i.e., unilamellar) vesicles that are less than 100 nm in diameter (*42*). These can be created by hydrating a dried lipid film, which causes the lipids to spontaneously form multilamellar (i.e., multi-bilayer) vesicles (*43*). These vesicles can then be

broken into SUVs by sonication (*43*). Once the SUVs are formed, their solution is deposited over a clean hydrophilic surface, often glass (*43*). Now, the vesicles all settle to the bottom of the solution, their hydrophilic exteriors attracted to the hydrophilic surface (*43*). To maximize the number of lipids interacting with the surface, the SUVs then start to fuse with neighboring vesicles, and eventually unravel into a continuous planar bilayer (*43*).

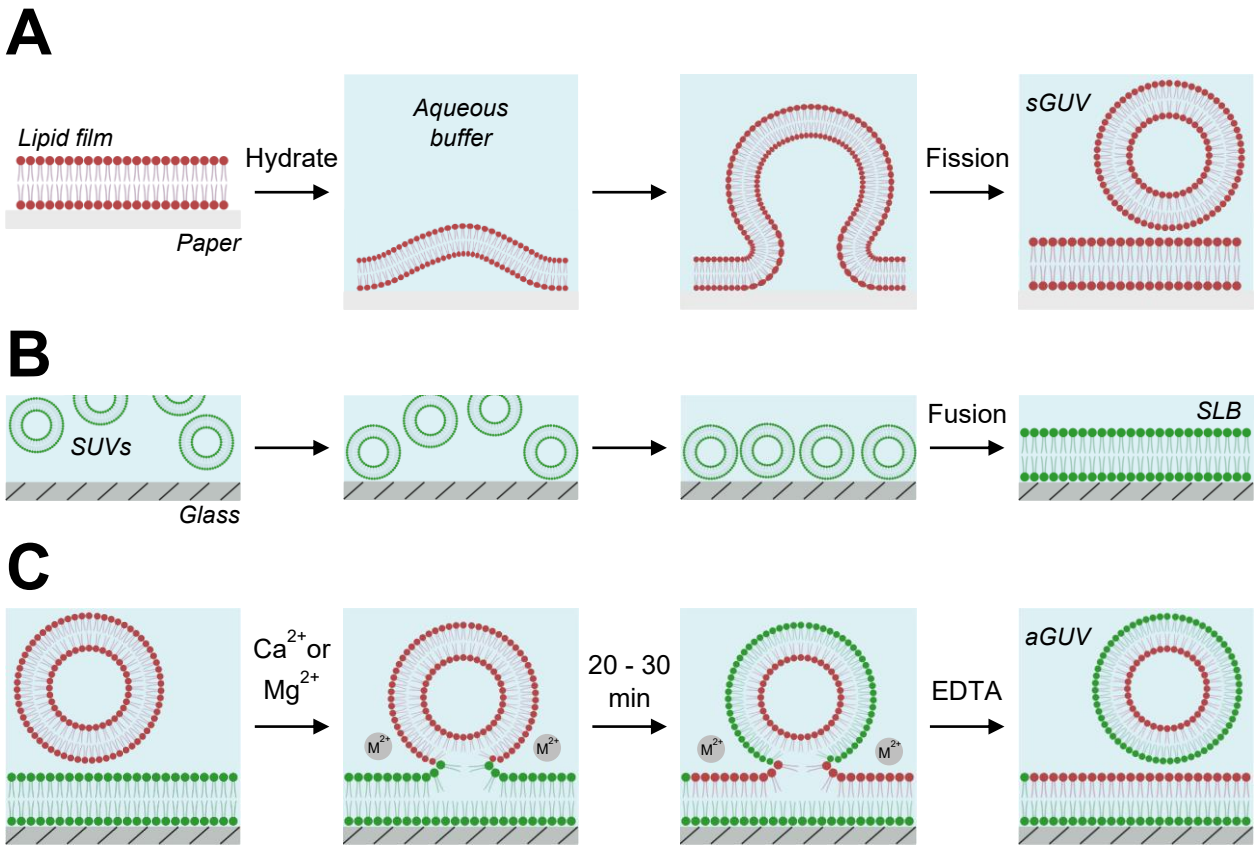

Figure 2. Formation of various model membranes. (*A*) Formation of sGUVs via the PAPYRUS method, where a paper surface containing a dried lipid film is hydrated, inducing fission of the lipids into sGUVs. (*B*) Formation of an SLB via the vesicle fusion method, where SUVs are deposited on a hydrophilic surface (e.g., glass), which then fuse and unravel to form a planar membrane. (*C*) Formation of aGUVs via the hemifusion method. First, hemifusion is induced between the outer membranes of sGUVs and an SLB by the addition of Ca^{2+} or Mg^{2+}. Once time has been given for lipid transfer to occur, fission is induced by the addition of excess EDTA.

Another specific type of model membrane is giant unilamellar vesicles (GUVs), meaning unilamellar vesicles with diameters in the micrometer range (*42*). These vesicles are frequently employed in studies due to being similar in size and form to key biological membranes, like the eukaryotic PM. GUVs may be symmetric (denoted sGUVs) or asymmetric (denoted aGUVs), meaning they do not or do possess vertical asymmetry respectively. sGUVs can be prepared through many different procedures. A more recent one is the paper-abetted lipid hydration in

aqueous solutions (PAPYRUS) method, which is shown in Figure 2A. This procedure involves first depositing a dried lipid film on a sheet of paper (*44*). This paper may be chromatography paper, filter paper, or tracing paper, though importantly, it must have a nanostructure consisting of a network of nanometer-scale cellulose fibers (*44, 45*). Once the lipid film is on the paper, it is hydrated, which results in fissioning of the film into sGUVs in solution (*44*). This process is proposed to occur through the initial budding of the film upon hydration, followed by the progressive growth of these buds (potentially fusing with neighboring buds) until they eventually fission into free vesicles (*45*). These buds presumably form in the first place due to the nanofibril structure of paper making the formation spontaneous, which is supported by thermodynamic models (*45*). The PAPYRUS protocol works best when the sGUVs are formed in an aqueous solution with minimal ions, as ions seem to interfere with the process in a manner that leads to a lesser yield of quality sGUVs (*44*). However, these issues can be overcome by modifying the procedure. In this new protocol, the lipids are first hydrated with a low ionic strength solution, then after 10 minutes, the mixture is brought up to the desired ionic strength by adding a concentrated ion solution (*44*). Doing so does not seem to induce osmotic stress of the forming vesicles, and yields sGUVs with no quality issues (*44*).

In comparison to the methods available for sGUVs fabrication, those available for aGUV preparation are much more limited. One method involves preparing a donor and acceptor population of vesicles that differ in lipid composition, then using cyclodextrin to mediate lipid transfer from the outer leaflets of donor vesicles to those on acceptor vesicles (*12*). This method can produce fairly consistent aGUVs if the donor vesicles are added in excess, which results in most or all of the lipids in acceptor vesicles' outer leaflets getting swapped (*12*). However, it is quite difficult to separate the cyclodextrin from the resulting aGUVs after the fabrication (*13*), making this method unideal. A different aGUV preparation method involves preparing a surfactant monolayer of lipids at an organic-aqueous boundary, then adding new lipids to the monolayer to convert it into a bilayer (*11*). The bilayer is then centrifuged to fission it into vesicles (*11*). This protocol can make aGUVs if the lipids in the initial monolayer differ from those added later, but the resulting vesicles are limited to only a few micrometers in diameter (*11*), which is not ideal when trying to model larger membranes (e.g., the eukaryotic PM).

The limited nature of these aGUV preparation methods is unfortunate, since aGUVs simulate biological members more accurately than other model membranes on account of being asymmetric, making them a more desirable system to work with. Thankfully, a new method for fabricating aGUVs published by Enoki et al. (*14*) addresses many of the issues seen in other aGUV preparation methods. This procedure is diagrammed in Figure 2C, and involves first adding sGUVs to an SLB. Next, Ca^{2+} is added to induce hemifusion between the membranes, which refers to the fusion of the outer sGUV leaflets with the outer SLB leaflet. This process is presumably enabled by the Ca^{2+} ions positioning themselves between the membranes, shielding their surface charges to allow the outer leaflets to touch. In the hemifused state, lipids are able to travel between the outer leaflets of the membranes. Since the SLB is much larger than the sGUVs, given enough time, the lipids in the outer leaflets of hemifused sGUVs should fully exchange with those on the SLB.

Therefore, in the hemifusion protocol, a period of time is given after the cation addition for lipid exchange, followed then by the addition of excess EDTA. This EDTA chelates the cations, inducing fission of the vesicles back into solution, presumable as a result of the cations no longer being present between the membranes to shield charge repulsions. These freed vesicles are, in theory, aGUVs with an inner leaflet composition equal to their initial sGUV composition, and an outer leaflet composition equal to the SLB composition. This hemifusion method has been used to successfully create aGUVs containing solely PC lipids (*14*), though it remains unknown if it can be used to make those containing different lipids, such as PS. Interestingly, preliminary work by Trevor Paratore (personal communication) shows that Mg^{2+} can be used to initiate hemifusion as an alternative for Ca^{2+}, though it is unknown how this substitution would affect the hemifusion process when working with PS-containing membranes.

2.4 Hypothesis

This study hypothesizes that the hemifusion method for aGUV preparation developed by Enoki et al. (*14*) can be adapted for the fabrication of PS-containing aGUVs. If this hypothesis is correct, the hemifusion method could serve as a reliable method for preparing PS-containing aGUVs, which could then be used in future experiments to study the interactions of PS (e.g., its binding interactions with proteins, the registration interactions PS domains may have with other membrane domains). This hypothesis was tested by applying the hemifusion method with PS-containing SLBs, then evaluating the resulting aGUVs via fluorescence microscopy.

3. Methodology

3.1 Materials

Nunc Lab-Tech II 4-well chambered coverglasses were purchased from Thermo Fisher (Waltham, MA). Commercial artist-grade tracing paper was purchased from Amazon (Seattle, WA). Liquinox was obtained from Alconox (White Planes, NY). Sodium chloride, potassium chloride, calcium chloride, magnesium chloride, disodium ethylenediamine tetraacetic acid (Na_2EDTA), 4-(2-hydroxyethyl)-1-piperazineethanesulfonic acid (HEPES), sucrose, and glucose were obtained in high purity grades either through Fisher Scientific (Fairlawn, NJ) or Sigma Aldrich (St. Louis, MO). HPLC grade chloroform, ethanol, isopropanol, and methanol were also obtained through Fisher Scientific (Fairlawn, NJ). Deionized water (18.2 MΩ-cm) was obtained using a RODI (Aztec, NM) high-purity water system.

1,2-dioleoyl-sn-glycero-3-phosphocholine (DOPC), 1-palmitoyl-2-oleoyl-sn-glycero-3-phosphocholine (POPC), sodium 1-palmitoyl-2-oleoyl-sn-glycero-3-phospho-L-serine (POPS), and ammonium 1-palmitoyl-2-(dipyrromethene boron difluoride)undecanoyl-sn-glycero-3-phospho-L-serine (TF-PS) were purchased from Avanti Polar Lipids (Alabaster, AL), while 1,1-dioctadecyl-3,3,3,3-tetramethylindodicarbocyanine 4-chlorobenzenesulfonate (DiD) was purchased from Invitrogen (Waltham, MA). Each reagent was obtained in powder form and used as received. A DiD stock solution was prepared by dissolving DiD powder in ethanol, while lipid stock solutions were dissolved in a solution of 2:1 chloroform:methanol (v:v). All stock solution was stored at -20 °C. The concentration of the fluorophore (DiD and TF-PS) stock solutions was determined using the Beer-Lambert relationship, approximated from absorbance measurements in methanol at 646 nm and 496 nm, respectively, and the corresponding extinction coefficients (ε). The ε of DiD was obtained from the reagent lot's certificate of analysis (ε = 250000 $M^{-1}cm^{-1}$), while the ε of TF-PS was taken from the literature (ε = 97000 $M^{-1}cm^{-1}$; *14*). These measurements were collected on a Thermo Fisher Scientific Evolution 300 UV-Visible spectrophotometer. Lipid stock concentrations were determined using an inorganic phosphate assay (*46*).

3.2 Buffer Preparation

Table 1 lists the compositions of all buffers that were used throughout this study. Buffers A through F are referred to as "low salt" buffers while buffers A_s through F_s are "high salt" buffers. Low salt buffers use lower-than-physiological concentrations of salts (NaCl and KCl), while high salt ones use physiological levels. The osmolality of low salt buffers was checked daily using an osmometer (The Advanced Micro Osmometer, Model 3300) and adjusted to within ± 2 mOsm/kg of each other by adding small volumes of DI water or 1 – 2 M NaCl. However, in the case of buffer E and F, either 1 M sucrose or glucose were used in place of NaCl respectively.

Table 1. Buffer compositions

Name	Composition
Buffer A	65 mM NaCl, 35 mM KCl, 25 mM HEPES, pH = 7.4
Buffer B	20 mM $MgCl_2$, 35 mM NaCl, 35 mM KCl, 25 mM HEPES, pH = 7.4
Buffer B’	11 mM $MgCl_2$, 42 mM NaCl, 42 mM KCl, 25 mM HEPES, pH = 7.4
Buffer C	20 mM $CaCl_2$, 35 mM NaCl, 35 mM KCl, 25 mM HEPES, pH = 7.4
Buffer C’	11 mM $CaCl_2$, 42 mM NaCl, 42 mM KCl, 25 mM HEPES, pH = 7.4
Buffer D	20 mM Na_2EDTA, 35 mM NaCl, 35 mM KCl, 25 mM HEPES, pH = 7.4
Buffer E	200 mM sucrose, 5 mM HEPES, pH = 7.4
Buffer F	200 mM glucose, 5 mM HEPES, pH = 7.4
Buffer G	500 mM NaCl, 20 mM citrate, pH = 4.0
Buffer A_s	100 mM NaCl, 100 mM KCl, 25 mM HEPES, pH = 7.4
Buffer B_s	20 mM $MgCl_2$, 100 mM NaCl, 70 mM KCl, 25 mM HEPES, pH = 7.4
Buffer B_s’	11 mM $MgCl_2$, 108 mM NaCl, 76 mM KCl, 25 mM HEPES, pH = 7.4
Buffer C_s	20 mM $CaCl_2$, 100 mM NaCl, 70 mM KCl, 25 mM HEPES, pH = 7.4
Buffer C_s’	11 mM $CaCl_2$, 108 mM NaCl, 76 mM KCl, 25 mM HEPES, pH = 7.4
Buffer D_s	20 mM Na_2EDTA, 100 mM NaCl, 70 mM KCl, 25 mM HEPES, pH = 7.4
Buffer E_s	100 mM sucrose, 100 mM NaCl, 50 mM KCl, 25 mM HEPES, pH = 7.4
Buffer E_s’	2 M NaCl, 1 M KCl, 500 mM HEPES, pH = 7.4
Buffer F_s	100 mM glucose, 100 mM NaCl, 50 mM KCl, 25 mM HEPES, pH = 7.4

3.3 sGUV Preparation

sGUVs were prepared using the PAPYRUS method with tracing paper as described by Pazzi et al. (*45*). In brief, a rectangular piece of tracing paper was first cleaned by submerging it in chloroform for 30 minutes, gently stirring the mixture every 10 minutes. This process was then repeated with a fresh volume of chloroform, after which it was repeated again with DI water. Next, the paper was dried in a vacuum oven. Once dry, a 6.35 mm diameter circular cutout was removed from the paper, and coated with a 10 µL solution containing 0.5 to 1 mM lipids dissolved in 2:1 (v:v) chloroform:methanol at the same mole ratio as the desired sGUVs. After applying this mixture, the cutout was dried in a vacuum oven. Next, it was placed in the bottom of a well on a microwell plate. If the sGUVs were to be prepared in low salt buffer, 150 µL buffer E was added to the well,

causing vesicles to bud from the dried lipid film on the paper and into solution. The resulting sGUVs were collected 2 hours later.

For sGUVs being prepared in high salt buffer, 142.5 µL 105 mM sucrose was first added to the well containing the paper cutout, followed by 7.5 µL buffer E_S' 10 minutes later, giving the solution the composition of buffer E_S. The sGUVs were then collected after 110 minutes.

To collect sGUVs after their formation, a pipette with a wide orifice tip was used to mix the solution in the well by aspirating and dispensing 100 µL of it 6 times. The solution was then removed. If the sGUVs were prepared in high salt buffer, the osmolality of their collected solution was then measured with an osmometer (The Advanced Micro Osmometer, Model 3300). Any buffers later added to these sGUVs were adjusted to within ± 2 mOsm/kg this reading using the same protocol as described for the low salt buffers.

sGUV solutions were used for experiments on the day of preparation and never reused. Circular paper cutouts were never reused, but cleaned pieces of paper were reused to make cutouts until a week after the cleaning.

3.4 Coating of Coverglasses

sGUVs were imaged in chambered coverglasses (i.e., chamber well plates with coverglass bottoms) which were coated with bovine serum albumin (BSA) to prevent the vesicles from sticking to the glass. To perform this coating on a chambered coverglass, it was first cleaned by rinsing its chambers with DI water three times, followed by ethanol two times, isopropanol once, then ethanol once. This rinsing was then repeated, ending with a final 3 rinses of DI water. Next, the coverglass was sonicated for 15 minutes in dilute Liquinox detergent (around 2% (w/v) in DI water) heated to 69 °C in a water bath sonicator (Branson 1510 Ultrasonic Cleaner). Once done, the coverglass was rinsed with DI water 12 times, followed by ethanol two times, isopropanol once, then ethanol once. This rinsing was then repeated with a final 12 rinses of DI water. Now sufficiently clean, the coverglass was dried down under N_2 gas and primed for BSA coating by filling each chamber with 0.1 M NaCl. After 40 minutes, 0.1 M NaCl was replaced with 1 mg/mL BSA in 0.1 M NaCl at pH = 5.0 to apply the BSA coating. After 3 or more hours, the coverglass was rinsed with DI water 12 times to remove excess BSA not bound to its surface.

BSA-coated coverglasses were used within two days of preparation. When not in use, these coverglasses had their chambers filled with DI water. BSA-coated coverglasses were never reused, but coverglasses used to prepare SLBs were reused to make BSA-coated ones.

3.5 SLB Preparation

SLBs were fabricated in chambered coverglasses using the vesicle fusion method first described by Brian and McConnell (*43*). In this procedure, SUVs were first prepared by creating a 1 mM lipid mixture in 2:1 (v:v) chloroform:methanol with the lipids at the same mole ratios as the desired

SLB. This solution was then dried down under N_2 and resuspended in buffer G to form multilamellar vesicles. Next, the multilamellar vesicles were converted into SUVs by first freezing the suspension in liquid N_2 six times, thawing it in a warm water bath after each freezing. Then, the suspension was sonicated using a tip sonicator (Sonics Vibra-Cell VCX130 Ultrasonic Processor), where an amplitude of 50% was applied to the vesicles in 15-second pulses (15 seconds on, 15 seconds off) for 30 minutes. The resulting SUVs were then diluted 5x in buffer G.

Before using the SUVs to form the SLBs, an unused chambered coverglass was first cleaned using the same method as described for the BSA-coated coverglasses. But in this case, after drying the cleaned coverglass down with N_2, it was plasma cleaned for one minute and 20 seconds using a Mercator Control Systems LF-5 Plasma System with O_2 gas. Immediately after plasma cleaning, 1 mL of the diluted SUVs was added to each chamber to begin SLB formation. In this process, the SUVs in each chamber settle to the bottom and fuse to form a planar bilayer. In this case, the SUVs were kept in an acidic, high ionic strength buffer (buffer G) to help overcome electrostatic repulsions that would inhibit fusing.

After 40 or more minutes, the unfused remnants of vesicles were washed out of the coverglass by submerging it in 2.5 L of DI water and using a syringe to gently rinse each chamber two times with 10 mL DI water. Next, the coverglass was removed from the water, and liquid was gently removed from the top of each chamber to return their volumes to 1 mL. Finally, the water in each chamber was exchanged for either buffer A or buffer A_s depending on if the SLB was being prepared in low or high salt buffer respectively. To do so, 1 mL of the buffer was added to a chamber dropwise, then 1 mL was gently removed from a location in the chamber different than where the buffer was added. This process was repeated for each chamber 16 – 24 times, stopping once the chamber's osmolality was equal to the buffer ± 2 mOsm/kg, measured using The Advanced Micro Osmometer, Model 3300. SLBs were used immediately after being prepared, and never reused.

3.6 Monitoring of Domain Formation in SLBs

SLBs were prepared in low or high salt buffer with POPC/POPS/TF-PS (69.9/30/0.1 mol%) or DOPC/POPS/TF-PS (69.9/30/0.1 mol%). These were then imaged before and after the introduction of 3 mM Ca^{2+} or Mg^{2+} to the aqueous phase by the addition of 400 µL buffer C' or B', or 400 µL buffer C_s' or B_s' if the SLBs were in low or high salt buffer respectively. 50 µL buffer E (if in low salt buffer) or buffer E_s (if in high salt buffer) was added to the SLBs at the same time as the cations to mimic the conditions of hemifusion. For each SLB, images were taken every 20 minutes following the additions at the same locations on the SLB.

3.7 aGUV Preparation

aGUVs were prepared using an adapted form of the hemifusion method described by Enoki et al. (*14*). In this procedure, 50 µL DOPC/DiD (99.9/0.1 mol%) sGUVs in low or high salt buffer was

added to a chamber containing a DOPC/POPS/TF-PS (69.9/30/0.1 mol%) SLB in low or high salt buffer respectively. After waiting 10 minutes for the sGUVs to settle to the bottom of the chamber, hemifusion between the sGUVs and SLB was induced by adding 5.5 mM Ca^{2+} or Mg^{2+} to the chamber via the addition of 400 µL buffer C or B (if in low salt buffer), or buffer C_s or B_s (if in high salt buffer). After waiting 23 minutes for hemifusion and lipid exchange to occur between the membranes, fission of the GUVs from the SLB was induced by adding 6 mM EDTA to the chamber via the addition of 600 µL buffer D (for low salt buffer) or buffer D_s (for high salt buffer). After waiting 10 minutes for fission to complete, the resulting aGUVs were imaged.

3.8 Fluorescence Imaging

All GUVs and SLBs were imaged using a Zeiss LSM 510 confocal microscope. SLBs and aGUVs were imaged in the coverglasses they were prepared in, while sGUVs were imaged in BSA-coated coverglasses by adding 50 µL of the sGUVs to 550 µL buffer F or F_s if they were prepared in low or high salt buffer respectively. When imaging vesicles, only those with no deformities (e.g., multilamellarity, tubules, non-spherical morphology) were imaged. All GUV images were obtained by using a plan-apochromat 63x oil immersion objective, while SLB images were taken either with this lens, or a plan-apochromat 10x air objective. Unless otherwise specified, all GUV images were taken by capturing a single frame at the equator of the vesicle, and later processed by applying a Gaussian blur of radius 1. Meanwhile, all 63x lens images of SLBs were taken as Z-stacks, with the Z-slices spanning from right above to right below the membrane. All Z-stacks in this study were converted into composite 2D images, where each pixel in the image has the average intensity of all the Z-slices at that pixel. Certain Z-stacks of SLB domains were taken at a low detector gain, and later, digitally brightened to avoid image artifacts. All 10x lens images of SLBs were single frames that were digitally brightened as well.

3.9 Analysis of Fluorescence Intensities

Using the analysis method developed by Enoki et al. (*14*), the fluorescence intensities of aGUVs were compared to those of sGUVs to evaluate the amount of lipid exchange each aGUV underwent during hemifusion. This analysis first involved deriving an intensity value for the DiD and TF-PS emissions of each aGUV. To do so, ImageJ macros provided by Thais Enoki and Gerald Feigenson (personal communication; used in *14*) were used to find the maximum DiD and TF-PS emission intensity along a ray going from the center of the vesicle outwards. This measurement was repeated for 359 more rays, with each angled in a different manner such to capture all areas of the vesicle. The maximum intensities captured by each ray were then averaged together to get an average maximum DiD intensity and average maximum TF-PS intensity for the vesicle. Going forward, these values will be referred to as “DiD intensity” and “TF intensity” respectively. In addition to being found for each aGUV, the DiD or TF intensity was also found for sGUVs with a composition matching the theoretical inner or outer leaflet composition of the aGUVs respectively.

Before performing any further analysis with each vesicle's DiD or TF intensity, outliers were removed from the data set. An outlier was defined as a vesicle that had a DiD or TF intensity outside the range of their corresponding average DiD or TF intensity ± double the standard deviation. This average and standard deviation were taken from the vesicle's sample, meaning all data for vesicles of that type, depending on composition (i.e., aGUV, sGUV with DiD, or sGUV with TF-PS) and buffer composition (i.e., low or high salt buffer). An aGUV found to be an outlier for one intensity (DiD or TF) value but not the other was considered an outlier, and both intensities were completely discarded. As with this outlier removal, all future analyses were done separately for vesicles in low and high salt buffers, meaning intensities from vesicles in low salt buffer were never compared to those from vesicles in high salt buffer, and vice versa

A vesicle's DiD or TF intensity essentially represents the average emission intensity of DiD or TF-PS across it, which is chiefly dependent on the fraction of DiD or TF-PS in the vesicle. aGUVs that experienced full outer leaflet exchange with the SLB should have half the fraction of DiD and TF-PS as their sGUV counterparts, meaning their DiD and TF intensities should be half that of the sGUVs. This reasoning was used to determine which aGUVs experienced complete outer leaflet exchange. In this analysis, an aGUV was considered to have undergone this complete exchange if both of the following were true:

1. Its DiD intensity fell within the range of the halved maximum and halved minimum DiD intensity of the corresponding sGUVs
2. Its TF intensity fell within the range of the halved maximum and halved minimum TF intensity of the corresponding sGUVs

When both of these conditions are met, it means the aGUV gave a DiD and TF intensity that was in line with what is expected from a population of vesicles with half the DiD and TF-PS content as the sGUVs. An aGUV that met these criteria is referred to as a "range-passing" aGUV, while those that did not are "range-failing."

The DiD and TF intensities of the aGUVs were also used to find each vesicle's outer leaflet DiD % exchange and TF % exchange. These values equal the aGUV's DiD or TF intensity ($\boldsymbol{I_a}$) divided by the halved average DiD or TF intensity of the corresponding sGUVs ($\boldsymbol{I_c}$), expressed as a percent:

$$Exchange\ Percent = \frac{\boldsymbol{I_a}}{\boldsymbol{I_c}/2} \cdot 100\% \quad (1)$$

An aGUV having close to a 100% outer leaflet DiD % exchange and TF % exchange indicates that its DiD and TF intensities closely matched the halved average intensities for the sGUVs. This situation suggests that the aGUV underwent at least a mostly complete outer leaflet transfer.

4. Results

4.1 Domain Formation in SLBs

When preparing PS-containing aGUVs via the hemifusion technique with PS in the SLB, a potential issue is that the addition of divalent cations to induce hemifusion could also induce PS domain formation in the SLB. If this formation occurs before hemifusion, sGUVs may hemifuse to regions of the SLB containing domains, resulting in them becoming overly enriched in PS. To test the likelihood of this scenario occurring, a series of experiments were performed in which SLBs were imaged before and at various time points after the addition of Ca^{2+} or Mg^{2+}. Initially, SLBs composed of POPC/POPS/TF-PS (69.9/30/0.1 mol%) in low salt buffer were imaged across multiple locations before and after the addition of 3 mM Ca^{2+} or Mg^{2+} in the aqueous phase above the SLB to mimic the conditions used in a prior PS domain study (*9*). This experiment was performed four times with Ca^{2+} and twice with Mg^{2+}, with example data shown in Figure 3. No changes were seen in the SLBs following the addition of Mg^{2+}. Meanwhile, the SLBs gained PS domains after the addition of Ca^{2+}, as indicated by the appearance of high intensity spots (i.e., regions enriched in TF-PS). The first domains appeared 20 – 40 minutes after the addition, though new domains continued to form throughout the full duration of imaging (180 minutes after the addition). Domains were barely visible on images when first appearing, though progressively grew in size over time. All domains were roughly circular in shape with jagged edges.

After testing POPC/POPS/TF-PS (69.9/30/0.1 mol%) SLBs, the experiment was repeated, but with the POPC replaced with DOPC to match the SLB composition used for hemifusion later in this study. This iteration of the experiment was performed seven times with Ca^{2+} and twice with Mg^{2+} in low salt buffer, and once with Ca^{2+} and Mg^{2+} in high salt buffer. Figure 4 shows example low salt buffer data, while Figure 5 shows example high salt buffer data. In both cases, there was no change upon Mg^{2+} addition, but domain formation was observed after Ca^{2+} addition. As was seen in the POPC replicates, the first domains formed 20 – 40 minutes after the addition, with new domains appearing throughout the full duration of imaging. All domains progressively grew in size over time, starting barely visible. The domains in low salt buffer were shaped in the same manner as those in the POPC replicates, but those in high salt buffer consistently had a more wispy shape.

The domains formed in each of the experimental cases were further compared by quantifying their diameter and number. This data is shown in Table 2. For each case, the number of domains per area was determined by first counting the total number of domains 180 minutes after the Ca^{2+} addition across all the imaged locations of all replicates. This number was then divided by the sum of the area of the SLB in each location. The diameter of each domain was defined as the diameter of the smallest circle able to fully encase the domain. For all cases, the number of domains per area was within 2 mm^{-2} of each other, while the average domain diameters were all within ± one standard deviation of each other.

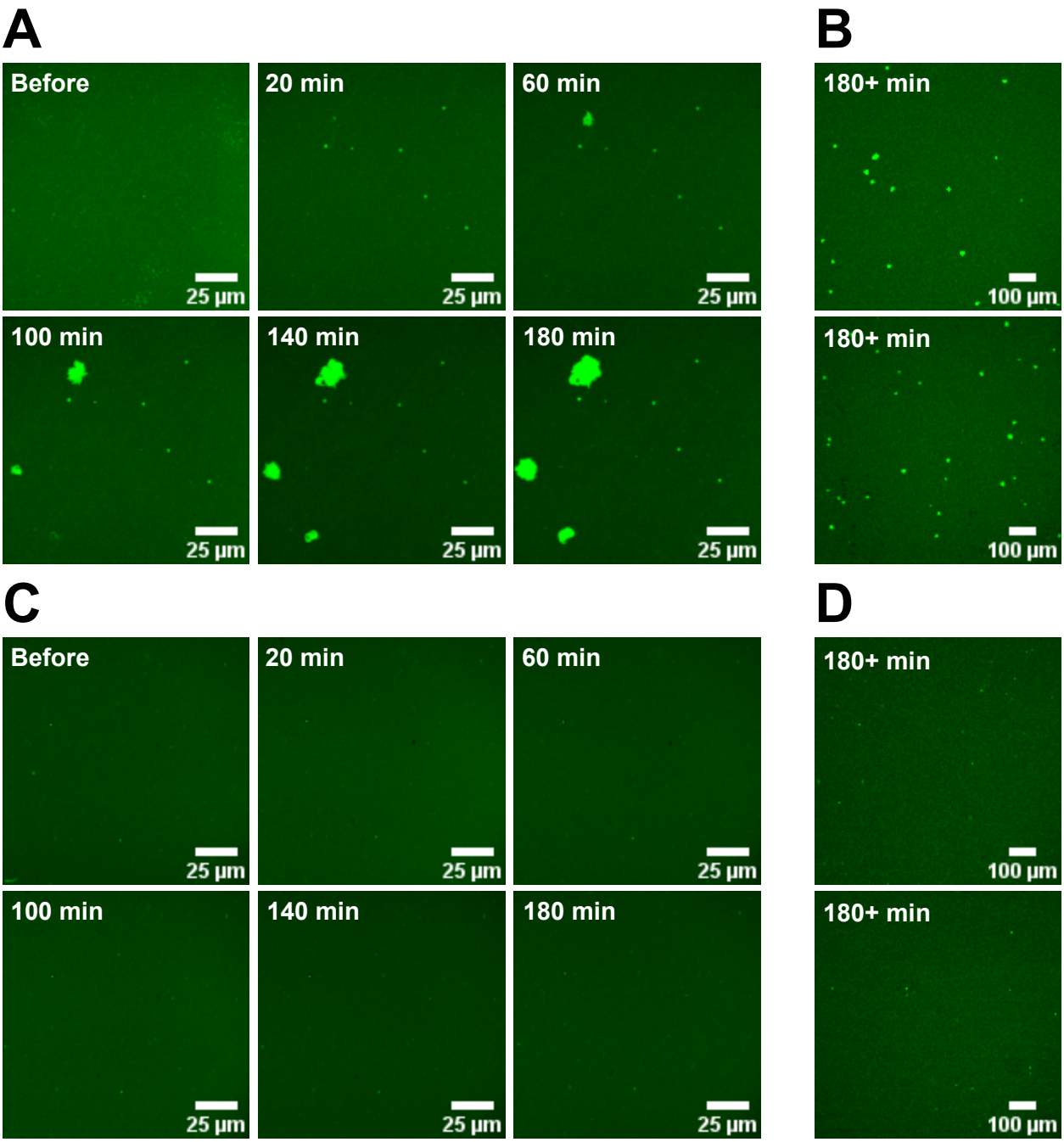

Figure 3. Effect of Ca^{2+} and Mg^{2+} on POPC/POPS/TF-PS (69.9/30/0.1 mol%) SLBs in low salt buffer. (*A*) 63x lens SLB images at the same location just before and at 20 to 180 minutes after Ca^{2+} is introduced to the aqueous phase. After the addition, the SLB is in 3 mM $CaCl_2$, 56 mM NaCl, 36 mM KCl, 7 mM sucrose, 24 mM HEPES, pH = 7.4 (*B*) 10x lens images of the SLB from panel A at two separate areas 180 or more minutes after adding Ca^{2+}. (*C*) & (*D*) Same as in panels A and B, but with 3 mM Mg^{2+} present in the aqueous phase in place of Ca^{2+}.

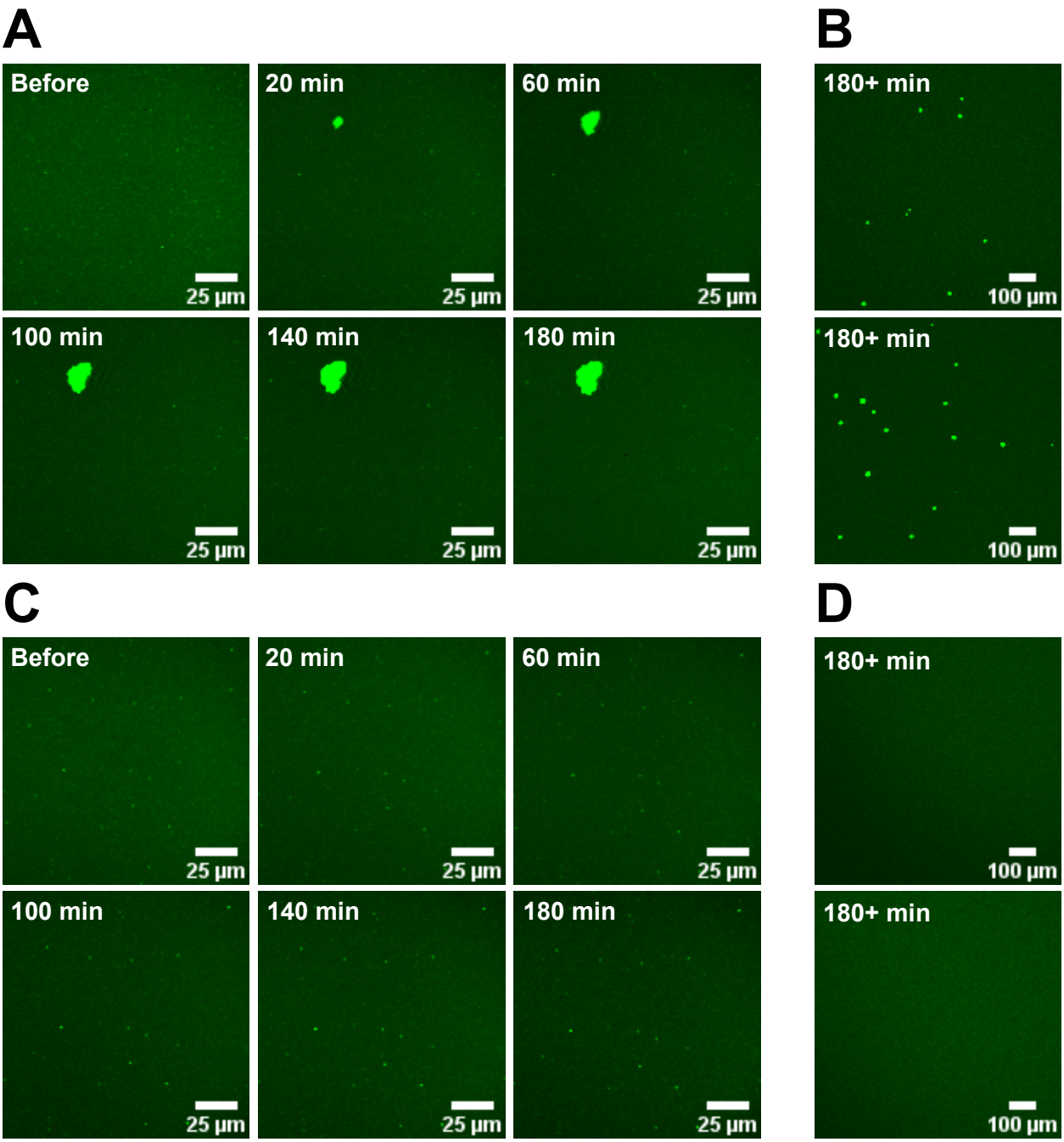

Figure 4. Effect of Ca^{2+} and Mg^{2+} on DOPC/POPS/TF-PS (69.9/30/0.1 mol%) SLBs in low salt buffer. (*A*) 63x lens SLB images at the same location just before and at 20 to 180 minutes after Ca^{2+} is introduced to the aqueous phase. After the addition, the SLB is in 3 mM $CaCl_2$, 56 mM NaCl, 36 mM KCl, 7 mM sucrose, 24 mM HEPES, pH = 7.4. Images were taken at a low detector gain and digitally brightened. (*B*) 10x lens images of the SLB from panel A at two separate areas 180 or more minutes after adding Ca^{2+}. (*C*) & (*D*) Same as in panels A and B, but with 3 mM Mg^{2+} present in the aqueous phase in place of Ca^{2+}.

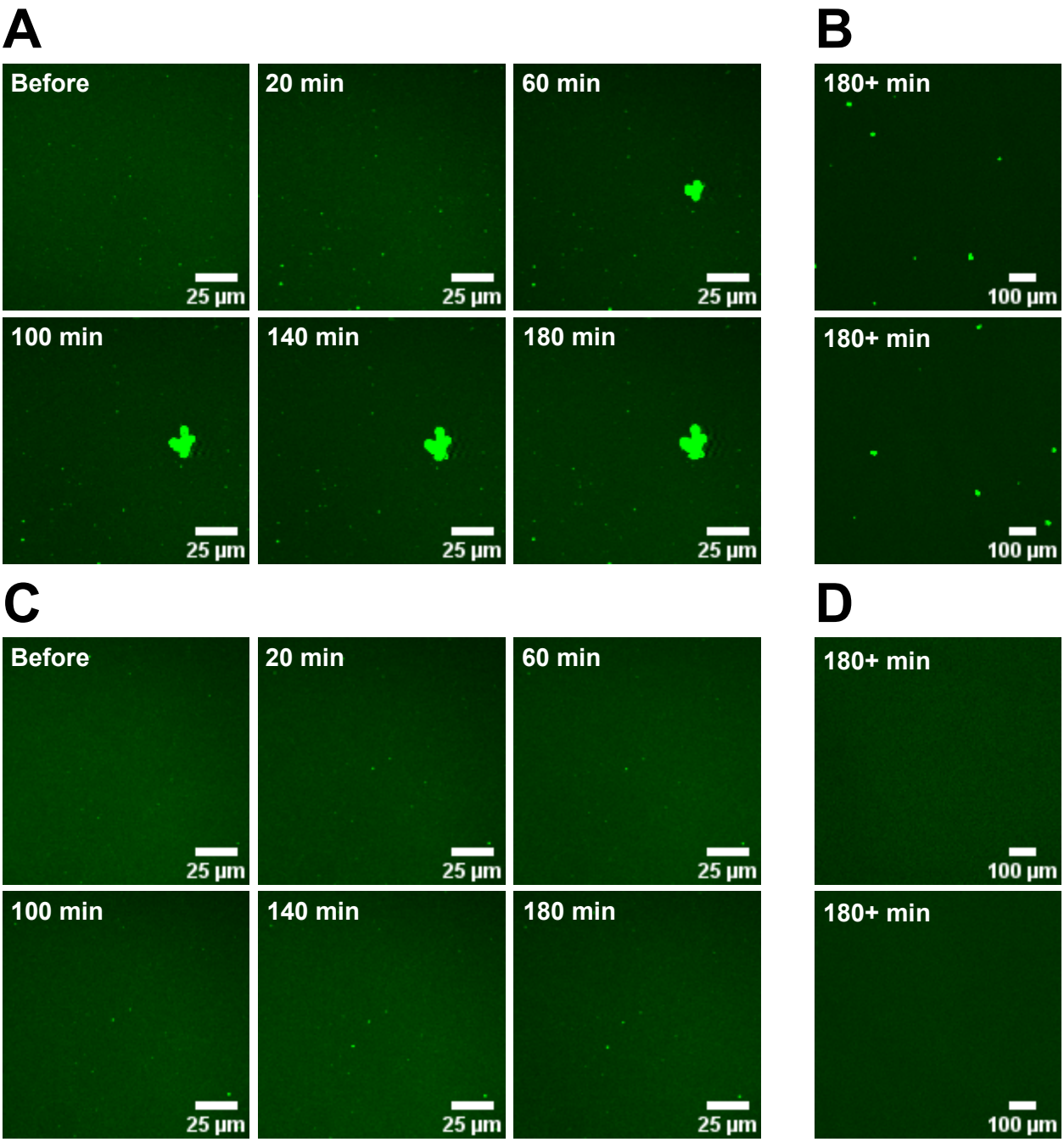

Figure 5. Effect of Ca^{2+} and Mg^{2+} on DOPC/POPS/TF-PS (69.9/30/0.1 mol%) SLBs in high salt buffer. (*A*) 63x lens SLB images at the same location just before and at 20 to 180 minutes after Ca^{2+} is introduced to the aqueous phase. After the addition, the SLB is in 3 mM $CaCl_2$, 102 mM NaCl, 92 mM KCl, 3 mM sucrose, 25 mM HEPES, pH = 7.4. Images were taken at a low detector gain and digitally brightened. (*B*) 10x lens images of the SLB from panel A at two separate areas 180 or more minutes after adding Ca^{2+}. (*C*) & (*D*) Same as in panels A and B, but with 3 mM Mg^{2+} present in the aqueous phase in place of Ca^{2+}.

Table 2. Size and number of domains in SLBs 180 minutes after 3 mM Ca^{2+} addition

SLB Composition	Buffer	Domains per Area (mm^{-2})	Avg. Domain Diameter ± SD (μm)
POPC/POPS/TF-PS (69.9/30/0.1 mol%)	low salt	11	11 ± 4
DOPC/POPS/TF-PS (69.9/30/0.1 mol%)	low salt	12	13 ± 6
DOPC/POPS/TF-PS (69.9/30/0.1 mol%)	high salt	13	12 ± 2

To more definitively test if domain formation would be present before hemifusion could take place, DOPC/POPS/TF-PS (69.9/30/0.1 mol%) SLBs were imaged before and after hemifusion with DOPC/DiD (99.9/0.1 mol%) sGUVs. Before images were taken right before the addition of sGUVs to the SLB while after images were taken right after the addition of EDTA. This experiment was performed twice with Ca^{2+} and Mg^{2+} in low and high salt buffer, with example data shown in Figure 6. Across all replicates, there were no changes in the SLBs after hemifusion.

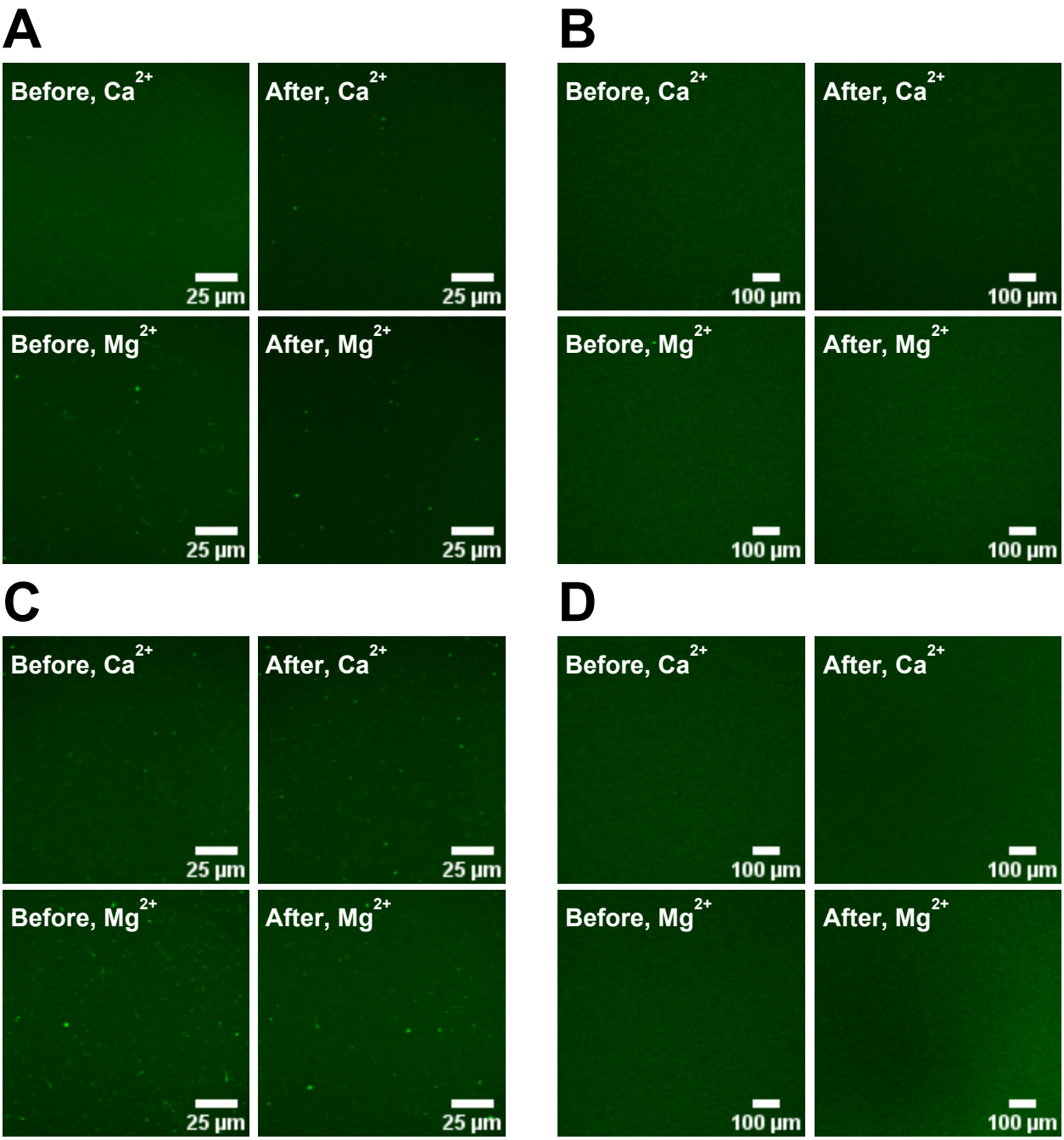

Figure 6. DOPC/POPS/TF-PS (69.9/30/0.1 mol%) SLBs before and after hemifusion. (*A*) 63x lens SLB images at the same locations before and after hemifusion in low salt buffer with Ca^{2+} or Mg^{2+}. The "before" image precedes the addition of the sGUVs while the "after" immediately follows the EDTA addition. Following this addition, the SLB is in 4 mM $CaCl_2$ (or $MgCl_2$), 6 mM Na_2EDTA, 49 mM NaCl, 34 mM KCl, 5 mM sucrose, 25 mM HEPES, pH = 7.4. (*B*) Same as panel A, but using the 10x lens. (*C*) & (*D*) Same as panels A and B, but in high salt buffer (4 mM $CaCl_2$ (or $MgCl_2$), 6 mM Na_2EDTA, 100 mM NaCl, 84 mM KCl, 2 mM sucrose, 25 mM HEPES, pH = 7.4).

4.2 Fabrication and Evaluation of aGUVs

To assess whether the hemifusion method for preparing aGUVs (*14*) could be used to fabricate those containing PS, the method was applied with DOPC/POPS/TF-PS (69.9/30/0.1 mol%) SLBs and DOPC/DiD (99.9/0.1 mol%) sGUVs. This procedure was performed eight times with Ca^{2+} and 18 times with Mg^{2+} in low salt buffer. It was performed four times with Ca^{2+} and four times with Mg^{2+} in high salt buffer. During four of the low salt buffer repeats, sGUVs with the same composition as the theoretical inner or outer aGUV composition were prepared and imaged. The same was done for three high salt buffer repeats.

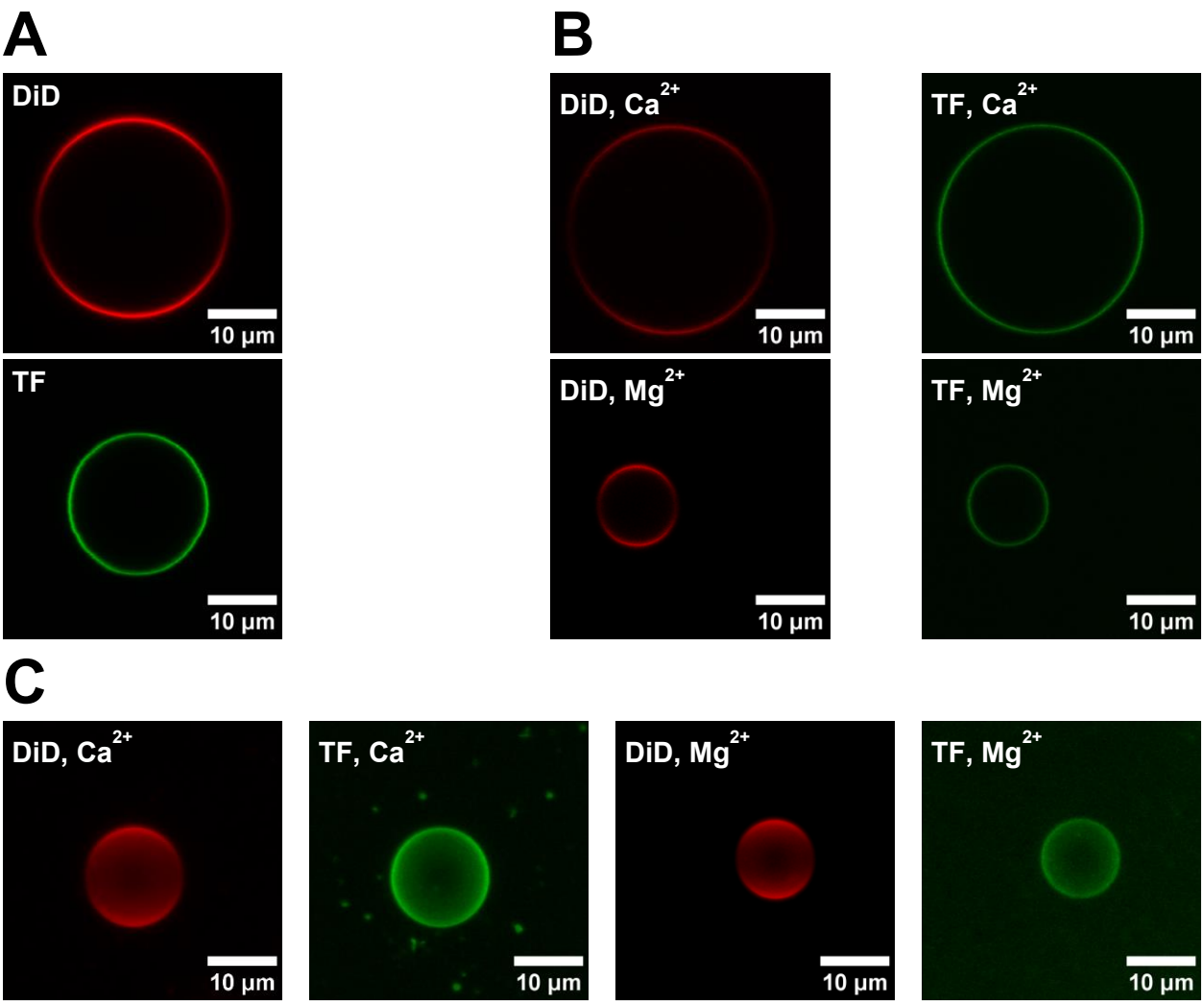

Figure 7. Images of sGUVs and aGUVs in low salt buffer. (*A*) Images of a DOPC/DiD (99.9/0.1 mol%) and DOPC/POPS/TF-PS (69.9/30/0.1 mol%) sGUV. sGUVs are in 180 mM glucose, 17 mM sucrose, 5 mM HEPES, pH = 7.4. (*B*) Images of aGUVs formed via hemifusion with Ca^{2+} or Mg^{2+}. For each aGUV, the DiD and TF channels are shown separately. aGUVs are in 4 mM $CaCl_2$ (or $MgCl_2$), 6 mM Na_2EDTA, 49 mM NaCl, 34 mM KCl, 5 mM sucrose, 25 mM HEPES, pH = 7.4. (*C*) Composite images of Z-stacks taken of a Ca^{2+}- and Mg^{2+}-formed aGUV in the same buffer as those in panel A.

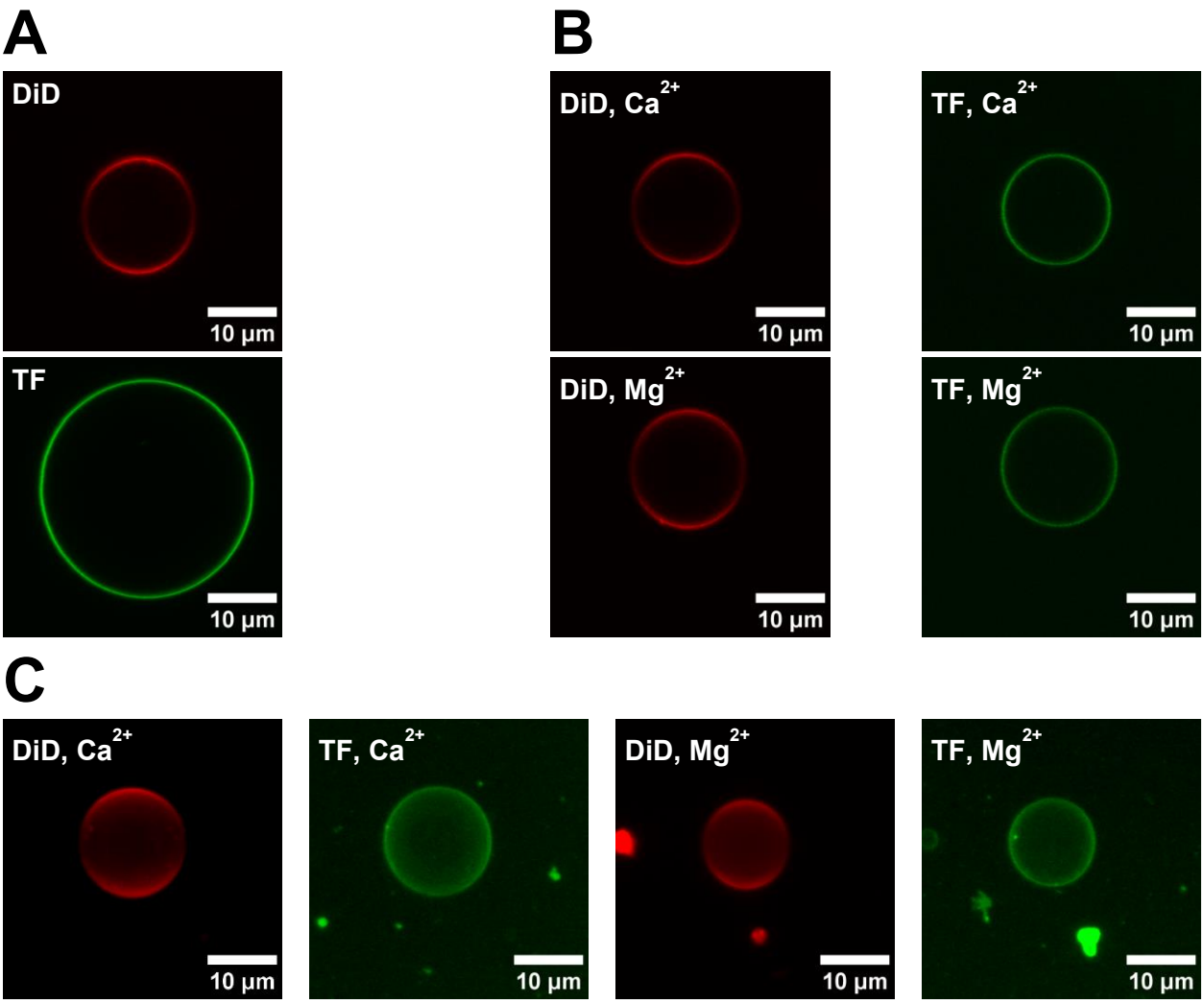

Figure 8. Images of sGUVs and aGUVs in high salt buffer. (*A*) Images of a DOPC/DiD (99.9/0.1 mol%) and DOPC/POPS/TF-PS (69.9/30/0.1 mol%) sGUV. sGUVs are in 90 mM glucose, 8 mM sucrose, 100 mM NaCl, 50 mM KCl, 25 mM HEPES, pH = 7.4. (*B*) Images of aGUVs formed via hemifusion with Ca^{2+} or Mg^{2+}. For each aGUV, the DiD and TF channels are shown separately. aGUVs are in 4 mM $CaCl_2$ (or $MgCl_2$), 6 mM Na_2EDTA, 100 mM NaCl, 84 mM KCl, 2 mM sucrose, 25 mM HEPES, pH = 7.4. (*C*) Composite images of Z-stacks taken of a Ca^{2+}- and Mg^{2+}-formed aGUV in the same buffer as those in panel A.

For all conditions, approximately 5 – 20% of GUVs underwent hemifusion to become aGUVs each time, as indicated by the them gaining TF fluorescence after the cation and EDTA additions. Figure 7 and 8 show example images of these aGUVs in low and high salt buffer respectively, as well as example images of the prepared sGUVs. The figures also show example Z-stacks of aGUVs created in each buffer composition with either cation. None of these Z-stacks had any major spots or holes, meaning the aGUVs are laterally homogenous with respect to each fluorophore. Note that all DiD images displayed greater intensity towards the top and bottom of the vesicle due to a polarization artifact, meaning this feature is not indicative of any lateral asymmetries.

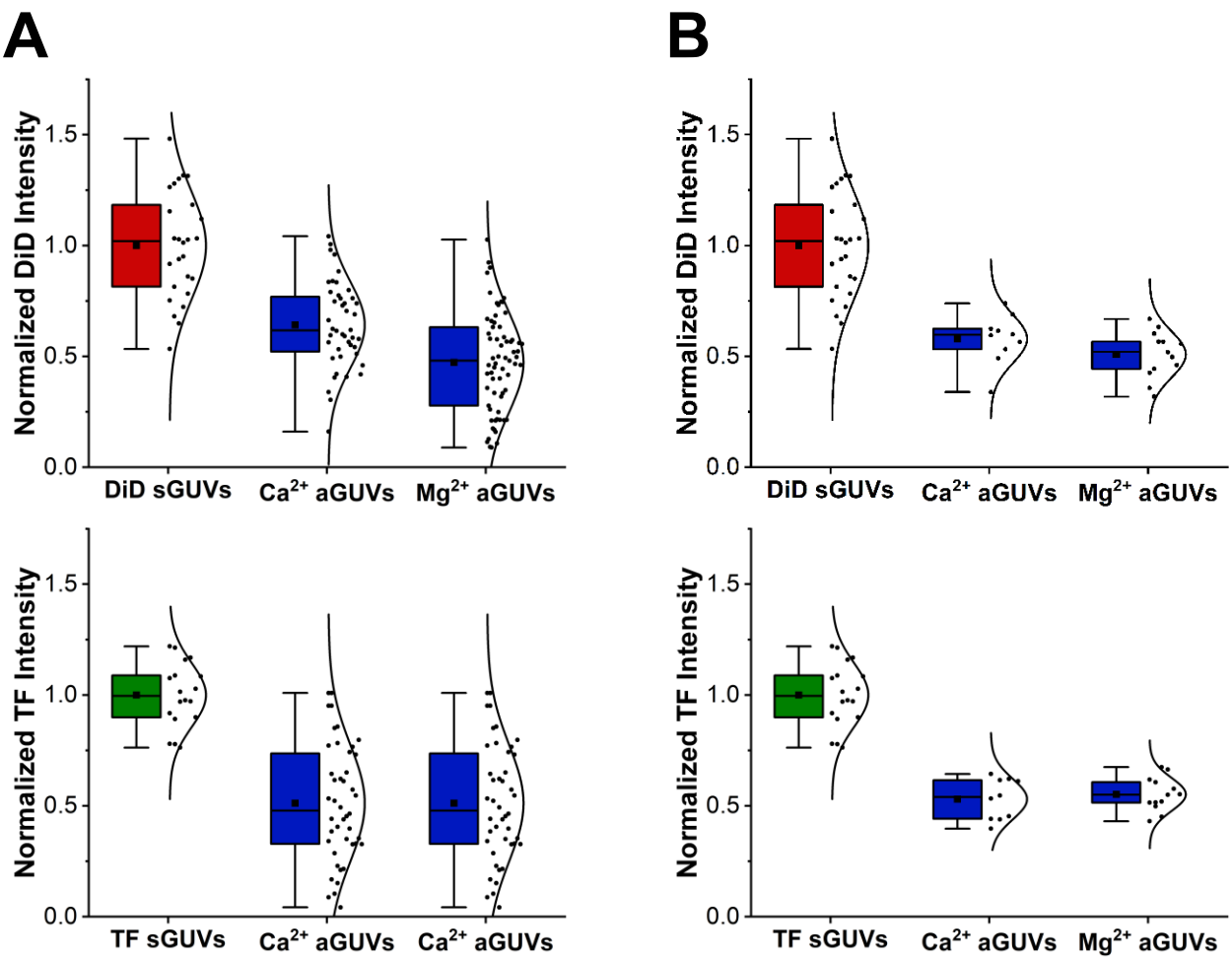

Figure 9. Intensity comparisons between sGUVs and aGUVs in low salt buffer. (*A*) Intensities of Ca^{2+}- and Mg^{2+}-formed aGUVs compared to those of sGUVs with compositions equal to the theoretical inner leaflet composition (DiD sGUVs) or theoretical outer leaflet composition (TF sGUVs) of the aGUVs. sGUVs are in 180 mM glucose, 17 mM sucrose, 5 mM HEPES, pH = 7.4 while aGUVs are in 4 mM $CaCl_2$ (or $MgCl_2$), 6 mM Na_2EDTA, 49 mM NaCl, 34 mM KCl, 5 mM sucrose, 25 mM HEPES, pH = 7.4. All intensities are normalized by the average of the corresponding sGUVs. Averages are shown as squares on each boxplot. (*B*) Same as panel A, but after removing all range-failing aGUVs.

To verify the composition of the prepared aGUVs, their DiD and TF intensities were compared to those of the corresponding sGUVs. This data is shown in Figure 9A for GUVs in low salt buffer, and in Figure 10A for those in high salt buffer. In all cases, the aGUVs gave average normalized DiD and TF intensities that were close to half the corresponding sGUV averages, ranging from 0.45 to 0.64 (0.50 meaning exactly half). This result demonstrates that the aGUVs have the expected composition on average. However, all aGUV distributions for normalized intensity gave considerable spread, each having a range of at least 0.55. This feature means that though the aGUVs give the expected composition on average, the exact composition of individual vesicles varies considerably. When comparing the spreads of different aGUV distributions, it is clear that

those from aGUVs in high salt buffer were tighter than those in low salt buffer, having ranges that were 1.1 to 3.2 times smaller than the corresponding low salt buffer distributions. Additionally, DiD intensity distributions were generally broader across both aGUVs and sGUVs, having ranges that were on average 1.5 times larger than the corresponding TF intensity distributions.

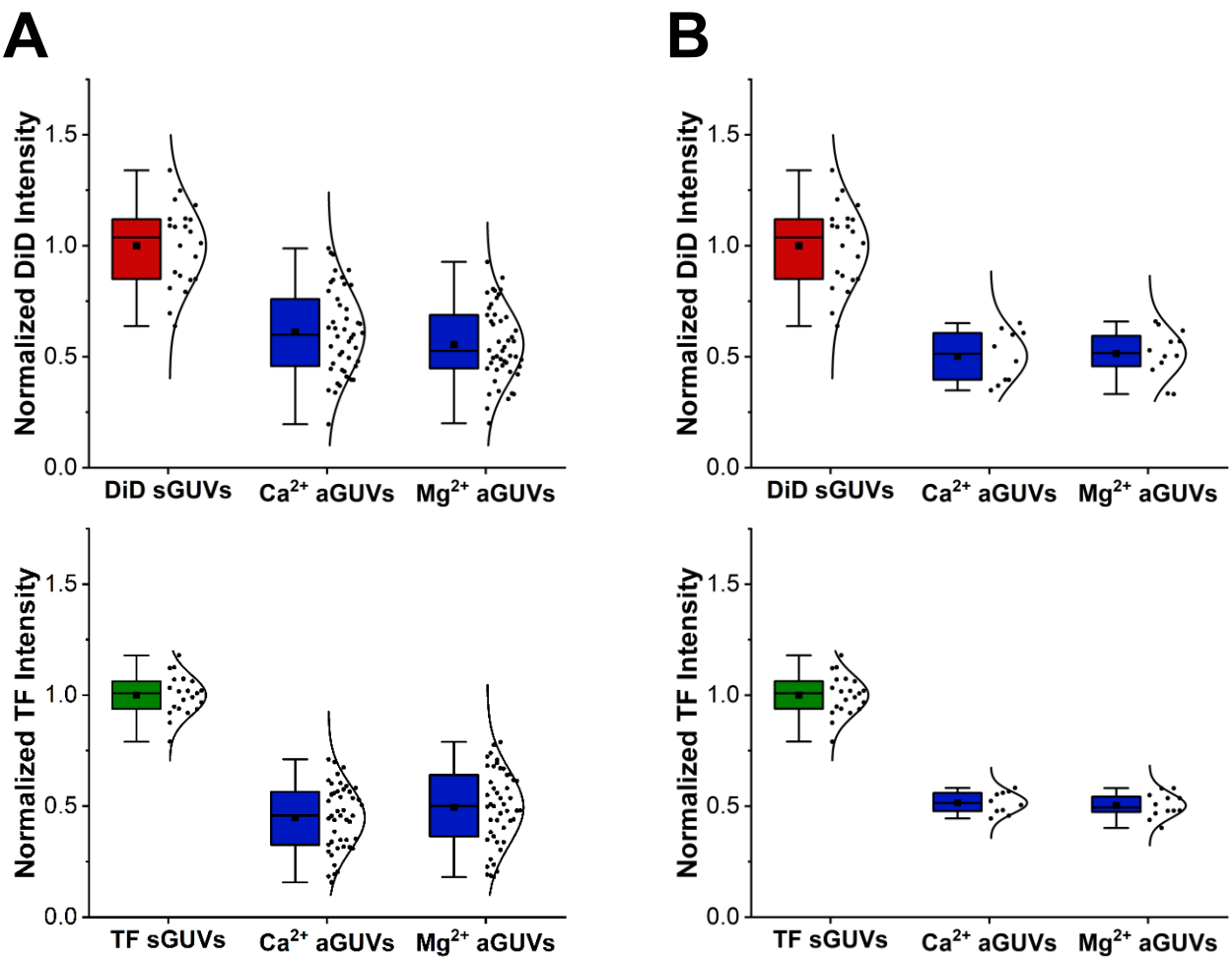

Figure 10. Intensity comparisons between sGUVs and aGUVs in high salt buffer. (*A*) Intensities of Ca^{2+}- and Mg^{2+}-formed aGUVs compared to those of sGUVs with compositions equal to the theoretical inner leaflet composition (DiD sGUVs) or theoretical outer leaflet composition (TF sGUVs) of the aGUVs. sGUVs are in 90 mM glucose, 8 mM sucrose, 100 mM NaCl, 50 mM KCl, 25 mM HEPES, pH = 7.4 while aGUVs are in 4 mM $CaCl_2$ (or $MgCl_2$), 6 mM Na_2EDTA, 100 mM NaCl, 84 mM KCl, 2 mM sucrose, 25 mM HEPES, pH = 7.4. All intensities are normalized by the average of the corresponding sGUVs. Averages are shown as squares on each boxplot. (*B*) Same as panel A, but after removing all range-failing aGUVs.

To select for aGUVs that were consistently the expected composition, aGUVs were filtered to remove all range-failing vesicles, meaning those with a DiD or TF intensity outside the range of the corresponding halved sGUV distribution. Doing so selected for aGUVs that had the expected

composition with the same degree of compositional variability as the sGUVs. When applying this filtering, 21% of aGUVs in low salt buffer and 24% in high salt buffer passed. Meanwhile, 22% of all aGUVs formed with Ca^{2+}, and 22% of all those formed with Mg^{2+} passed. The intensity distributions after applying this filtering are shown in Figure 9B and 10B for low and high salt buffer respectively. The average normalized intensities from these new distributions were even closer than before to being half of the corresponding sGUV averages, ranging from 0.50 to 0.58. Additionally, the new distributions were tighter than the corresponding unfiltered distributions, having ranges that were on average 3.1 times smaller than these unfiltered distributions. These results demonstrate that the filtered aGUVs are on average the expected composition, with very little variability between individual vesicles.

The intensities of each aGUV were compared to the average sGUV intensities to derive their outer leaflet DiD and TF % exchanges. Exchanges of 100% indicate that an aGUV has the expected intensity for that fluorophore given the theoretical composition. Therefore, an aGUV having 100% for both outer leaflet DiD and TF % exchange indicates that it is the expected composition. The exchanges for each aGUV are plotted in Figure 11 and 12 for those in low and high salt buffer respectively. For both the unfiltered and filtered aGUV data, data points were scattered across the plots, though centered at around (100, 100). There was no clear correlation between outer leaflet DiD and TF % exchange, though some trends were observed. In both low and high salt buffer, 2 – 3 times more Ca^{2+}-formed aGUVs had outer leaflet DiD % exchanges above 100% than below. This relationship indicates that the majority of these aGUVs have larger than expected DiD intensities (“expected” being determined by the aGUVs’ theoretical compositions). Table 3 shows the percent of aGUVs in each data set that had larger/lower than expected DiD or TF intensities, as determined by looking at their percent exchanges. In all other data sets, the percentages of aGUVs above/below the expected intensity were about equal.

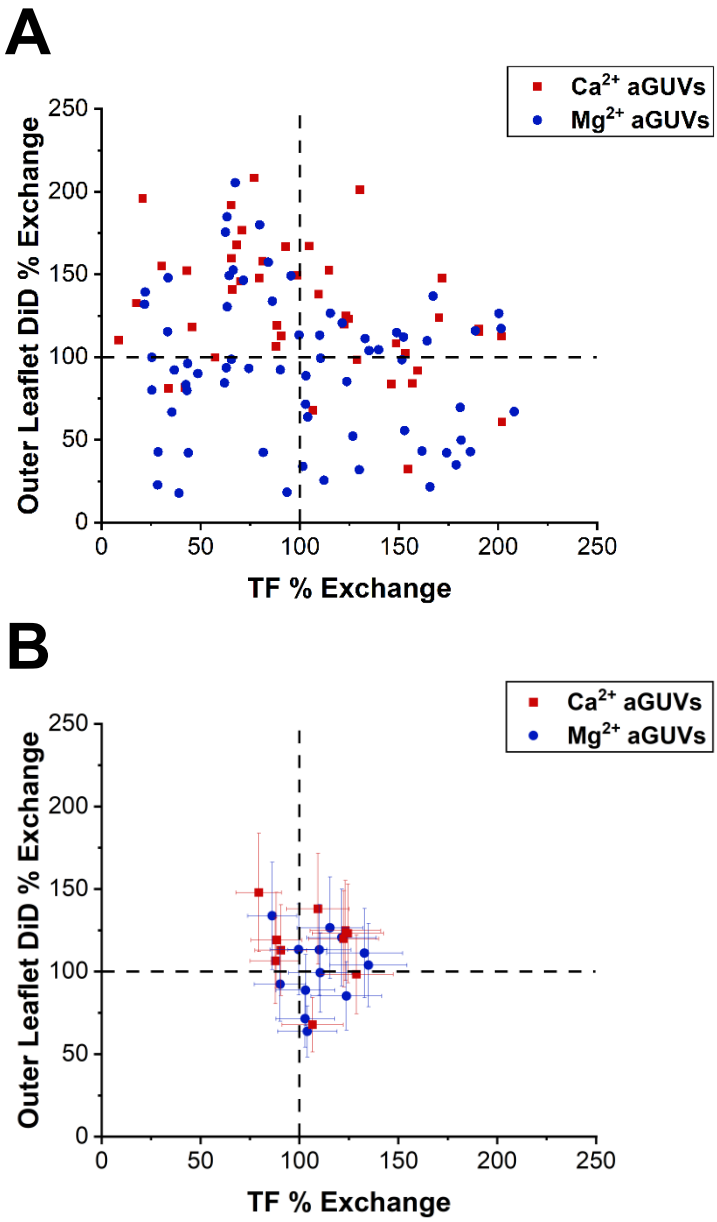

Figure 11. Exchange percent plots for aGUVs in low salt buffer. (*A*) Outer leaflet DiD % exchange vs TF % exchange for Ca^{2+}- and Mg^{2+}-formed aGUVs. aGUVs are in 4 mM $CaCl_2$ (or $MgCl_2$), 6 mM Na_2EDTA, 49 mM NaCl, 34 mM KCl, 5 mM sucrose, 25 mM HEPES, pH = 7.4. Error bars are omitted for clarity. (*B*) Same plot as in panel A, but after removing all range-failing aGUVs. Error bars are calculated via a propagation of uncertainty using standard deviations.

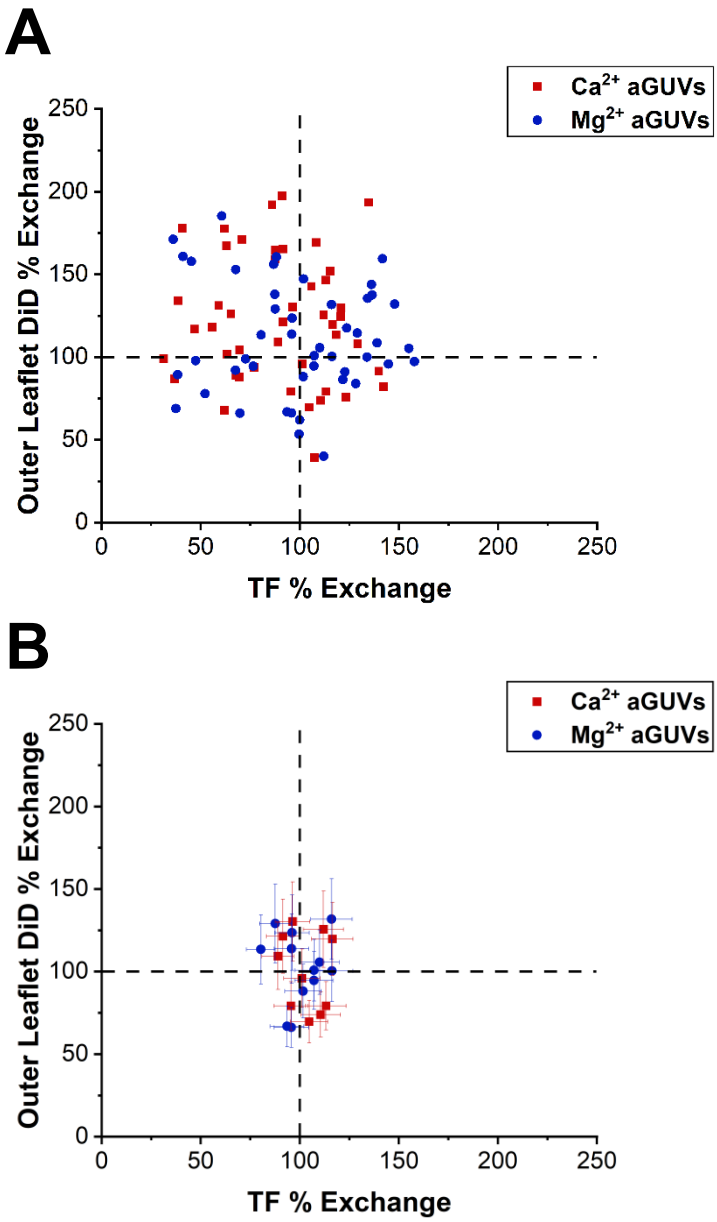

Figure 12. Exchange percent plots for aGUVs in high salt buffer. (*A*) Outer leaflet DiD % exchange vs TF % exchange for Ca^{2+}- and Mg^{2+}-formed aGUVs. aGUVs are in 4 mM $CaCl_2$ (or $MgCl_2$), 6 mM Na_2EDTA, 100 mM NaCl, 84 mM KCl, 2 mM sucrose, 25 mM HEPES, pH = 7.4. Error bars are omitted for clarity. (*B*) Same plot as in panel A, but after removing all range-failing aGUVs. Error bars are calculated via a propagation of uncertainty using standard deviations.

Table 3. Percent aGUVs* above/below expected intensities based on theoretical composition

Buffer	Cation	% Above (DiD Intensity)	% Below (DiD Intensity)	% Above (TF Intensity)	% Below (TF Intensity)
low salt	Ca^{2+}	77	23	48	52
low salt	Mg^{2+}	43	57	48	52
high salt	Ca^{2+}	67	33	42	58
high salt	Mg^{2+}	55	45	49	51

*Data from all aGUVs (before filtering) is used here.

To determine if vesicle size was influencing fluorescence data, the average diameter of the sGUVs and aGUVs was found, shown in Figure 13. On average, vesicles prepared in low salt buffer had diameters 1.6 times larger than those in high salt buffer. Additionally, in both low and high salt buffer, the sGUVs had diameters that were on average 1.8 times larger than the aGUVs. But in both buffers, the average sGUV and aGUV diameters were within one standard deviation of each other. Similarly, the average diameters for aGUVs that were range-passing and range-failing were within one standard deviation of each other, indicating that diameter is not correlated with aGUVs being of the expected composition. The relationship between vesicle size and fluorescence data is explored in greater detail in Appendix A.

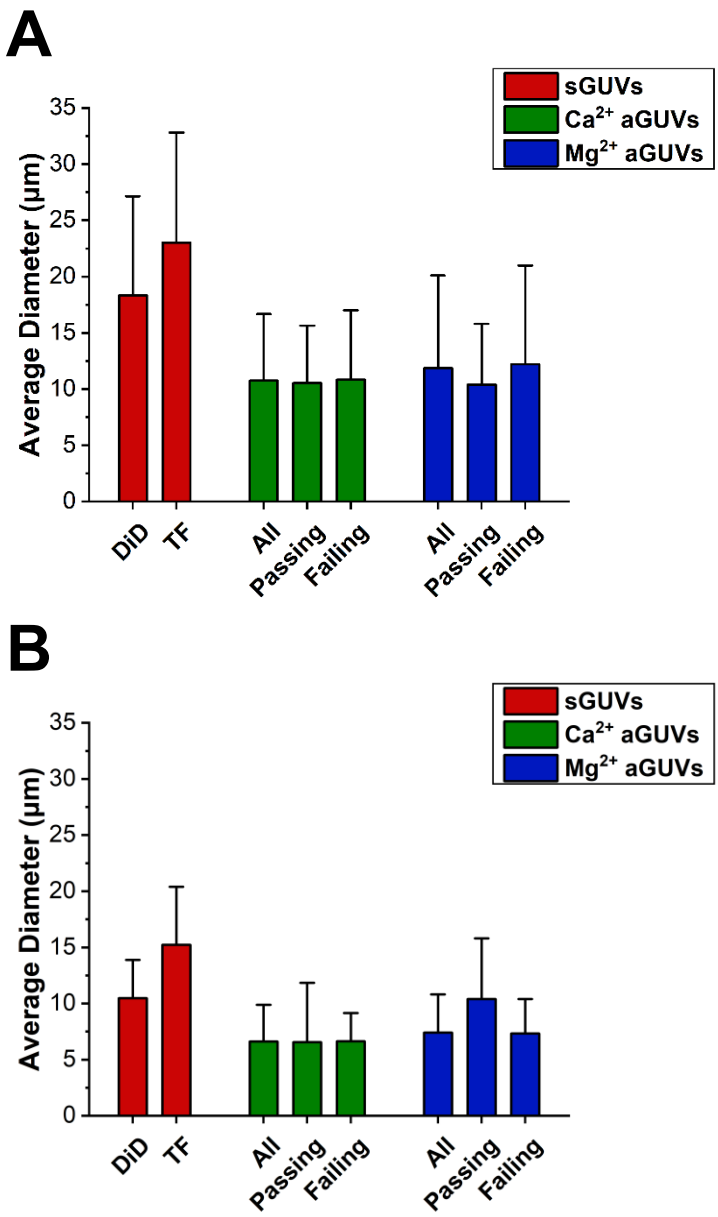

Figure 13. Diameter comparisons between sGUVs and aGUVs. (*A*) Average diameter of all Ca^{2+}- and Mg^{2+}-formed aGUVs, those that are range-passing, and those that a range-failing compared to that of sGUVs whose compositions match the theoretical inner leaflet composition (DiD sGUVs) or theoretical outer leaflet composition (TF sGUVs) of the aGUVs. Error bars show standard deviations. All vesicles are in low salt buffer (180 mM glucose, 17 mM sucrose, 5 mM HEPES, pH = 7.4 for sGUVs; 4 mM $CaCl_2$ (or $MgCl_2$), 6 mM Na_2EDTA, 49 mM NaCl, 34 mM KCl, 5 mM sucrose, 25 mM HEPES, pH = 7.4 for aGUVs). (*B*) Same as panel B, but for vesicles in high salt buffer (90 mM glucose, 8 mM sucrose, 100 mM NaCl, 50 mM KCl, 25 mM HEPES, pH = 7.4 for sGUVs; 4 mM $CaCl_2$ (or $MgCl_2$), 6 mM Na_2EDTA, 100 mM NaCl, 84 mM KCl, 2 mM sucrose, 25 mM HEPES, pH = 7.4 for aGUVs).

5. Discussion

Current methods available for the fabrication of PS-containing asymmetric model membranes are limited, so this study sought to derive a new method for the preparation of PS-containing aGUVs by adapting a technique published by Enoki et al. (*14*). In this procedure, Ca^{2+} is used to induce hemifusion between sGUVs and an SLB containing PS. Once hemifused, the sGUVs are able to exchange their outer leaflet lipids with those on the SLB, in theory giving these leaflets the same composition as the SLB. After time has been given for these transfers to occur, EDTA is used to induce fissioning of the GUVs (now aGUVs) from the SLB back into solution. This method was performed successfully in both a low and high salt buffer to obtain aGUVs with PS in the outer leaflet. It was also done successfully when using Mg^{2+} to induce hemifusion, which was tested as an alternative to Ca^{2+} (based on work by Trevor Paratore, personal communication) due to the ability of Ca^{2+} to cause PS domain formation. All of the fabricated aGUVs were intentionally "inside out" (i.e., while in the eukaryotic PM, PS resides in the inner leaflet of the bilayer, aGUVs were prepared to have PS in the outer leaflet). This property is advantageous, as it allows for the aGUVs to be used in future experiments to investigate interactions between PS and species in solution (e.g., proteins, inorganic cations). The aGUVs produced here were on average the expected composition as determined by fluorescence. However, the compositions of individual aGUVs varied significantly. Therefore, a data filtering method was created which selects for aGUVs with the expected composition. These aGUVs would be suitable for usage in future experiments due to their compositional consistency.

5.1 Domain Formation in SLBs

A potential issue when applying the hemifusion method for the fabrication of PS-containing aGUVs is that the divalent cations used could form PS domains in the SLB before hemifusion takes place. As a result, hemifusion would take place on a laterally heterogenous SLB, resulting in the composition of lipids transferred from this membrane to the sGUVs being different between vesicles (due to some sGUVs hemifusing at domains while others do not). In evaluating the likelihood of this issue occurring, the ability of divalent cations to form PS domains was first confirmed by reproducing an experiment performed by Neumann et al. (*9*). In this experiment, the researchers imaged POPC/POPS/TF-PS (69.9/30/0.1 mol%) before and after constantly flowing a gradient of 1 to 3 mM Ca^{2+} above the SLB via a microfluidic system. They observed that PS domains first formed in the 3 mM Ca^{2+} region 30 minutes after starting the flow, and 180 minutes after this start, the domains in this region had grown to an average diameter of 23 µm (standard deviation of 10 µm). When this experiment was repeated for this study, the same procedure was followed, but 3 mM Ca^{2+} was simply added above the SLB instead of flowing it over the membrane. Similar to the results obtained by Neumann et al., domain formation started 20 – 40 minutes after the addition, though the final domains had only an average diameter of 11 µm (standard deviation of 4 µm). This difference is likely a result of the constant flow of Ca^{2+} aiding in domain growth, as it ensures there remains a constant concentration of Ca^{2+} in the

aqueous phase as more and more Ca^{2+} binds the membrane. Overall, these results confirm that at least Ca^{2+} can form PS domains.

The Ca^{2+} domain formation experiment was later repeated, but using DOPC in place of POPC to confirm that these membranes (which were the same composition as those used in hemifusion) respond to Ca^{2+} in the same manner. These trials were done in low and high salt buffer, and like the POPC experiment, domain formation started 20 – 40 minutes after the Ca^{2+} addition in both cases. The average diameter and number of domains 180 minutes after the addition were also effectively the same as in the POPC experiment. Therefore, it does not seem like swapping POPC for DOPC or varying the buffer composition significantly impacts how the SLBs respond to Ca^{2+} in terms of domain formation. However, buffer composition may influence the morphology of these domains, as those obtained in high salt buffer consistently had a more wispy shape than those in low salt buffer.

To assess if the SLBs form domains in response to Mg^{2+} as is seen with Ca^{2+}, all of the experiments were repeated, but with Mg^{2+} instead of Ca^{2+}. In all cases, no domain formation was observed. This result suggests that Mg^{2+} does not form PS domains, though it could also mean that Mg^{2+} only forms nanodomains, which are not resolvable by the microscope. Nevertheless, this result is in line with fluorescence microscopy experiments performed by Haverstick and Glasser (*8*), in which no domain formation was seen 30 minutes after exposing PS-containing sGUVs to 2 mM Mg^{2+}. Though this result could again be due to Mg^{2+} only inducing nanodomain formation. Future studies using higher resolution techniques could be done to evaluate if these nanodomains exist, such as by using the self-quenching approach applied by Wen et al. (*47*) to detect phosphatidylinositol-4,5-bisphosphate nanodomain formation.

From the prior experiments, it was clear that Ca^{2+} can form domains in the SLBs, but it was unclear if these domains would form before hemifusion could take place. To evaluate this issue, SLBs were imaged in low and high salt buffer right before and after hemifusion. In all cases, no domains could be detected, suggesting that the domains form too slowly to appear before hemifusion. Therefore, it does not seem that domain formation by divalent cations is an issue when applying the hemifusion method to prepare PS-containing aGUVs.

5.2 Fabrication and Evaluation of aGUVs

The PS-containing aGUVs prepared in this study via hemifusion were evaluated for their composition in each leaflet by measuring the fluorescence intensity of fluorophores maintained in the inner leaflet (DiD), and those added to the outer leaflet (TF-PS). A limitation of this technique is that it only allows for the direct assessment of the fluorophores' fractions in each leaflet rather than the fractions of every lipid. However, if the fluorescence data for a vesicle indicates that it has the expected fraction of its fluorophores, it can be extrapolated that the other lipids must be in the vesicle at the expected fractions as well. Another limitation of this evaluation method is that it does not allow for the fluorescence signal in the inner and outer leaflets to be directly distinguished from each other. Therefore, a vesicle that has all of the fluorophore

molecules in one leaflet could appear compositionally equivalent to one with the same amounts of fluorophore segregated to separate leaflets. However, it can be assumed that TF-PS only exists in the outer leaflet based on quenching experiments performed by Enoki et al. (*14*) which showed that fluorophores added to a vesicle during hemifusion effectively only enter the outer leaflet. Though it is theoretically possible for these fluorophores to diffuse to the inner leaflet over time, this movement would likely take hours on account of the slow transverse diffusion of polar membrane lipids (*20, 25*), making this process irrelevant for this study.

All of the GUVs prepared in this study showed some levels of variability in composition as indicated by the variability in their fluorescence data. For the sGUVs, this variability is likely a result of the lipid film used to form the vesicles not being perfectly homogenous, or due to the lipids in the film not incorporating into vesicles at constant rates. DiD consistently gave more variable fluorescence data than TF-PS, which could indicate that DiD incorporates into sGUVs less consistently, leading to the DiD composition in sGUVs being more variable. This effect would then make the DiD composition in aGUVs more variable too, since these are prepared from DiD-containing sGUVs. Other potential sources of compositional variability in aGUVs are the hemifusion process occurring at an SLB region containing nanodomains, or the leaflet exchange not being fully complete before EDTA addition. It was observed that aGUVs fabricated in high salt buffer gave less variability than those in low salt buffer. This result could indicate that high salt buffer depreciates variability-causing factors (e.g., incomplete leaflet exchange), or it could be a result of the high salt buffer data set coming from fewer experimental repeats.

When filtering aGUVs to select for those with the expected composition, 22% of all vesicles made it through. The rate for just aGUVs formed with Ca^{2+} was equivalent to the rate for those formed with Mg^{2+}, indicating that which cation an aGUV was formed with does not impact the likelihood that it is the expected composition. The rate among aGUVs prepared in high salt buffer was slightly higher than the rate for those formed in low salt buffer (21% vs 24%), which could indicate that high salt buffer promotes the formation of compositionally correct aGUVs. However, the difference here is rather small, and therefore could be coincidental. Nevertheless, this difference does line up with the previous observation that aGUVs in high salt buffer were less compositionally variable, meaning they were more consistently around the expected composition. In all cases, the percentage of aGUVs passing filtering is smaller than what would be desirable. Future studies could look into modifying the hemifusion conditions to improve the pass rate. For example, if high salt buffer does promote the formation of aGUVs with the proper composition, doing the experiment in an even higher ionic strength buffer could further promote this effect. Performing the experiment at a different temperature may also promote this effect, though the hemifusion method has thus far only been tested at room temperature, so it is unknown. Alternatively, the pass rate may be improved by using a different divalent cation concentration during hemifusion or waiting less or more time before the EDTA addition. Enoki et al. (*14*) were able to get hemifusion with membranes containing just DOPC and fluorophores when using Ca^{2+} concentrations ranging from 3 – 7 mM and waiting times ranging from 20 – 30

minutes before EDTA addition. Therefore, trying different concentrations or times within these ranges may yield higher pass rates.

The relationship between exchange percents for aGUVs obtained in this study was notably different than those obtained by Enoki et al. (*14*) when preparing aGUVs in a low salt buffer with solely DOPC and fluorophores. They followed the same procedure as used here, though only used Ca^{2+} to induce hemifusion, while also varying the exact Ca^{2+} concentration (from 3 – 7 mM) and time before EDTA addition (from 20 – 30 minutes) across replicates. They observed a wide range of exchange percents across aGUVs as was seen in this study, though they also saw a strong increasing linear relationship between outer leaflet DiD % exchange and TF % exchange. Meanwhile, no correlation could be derived between the two exchange percents in this study. This difference could be due to the presence of PS in this study's membranes, or due to this study's use of more consistent hemifusion conditions (i.e., cation concentration and time before EDTA addition). However, it remains unclear how these factors would lead to this difference.

In their experiments, Enoki et al. (*14*) also did not observe the same trend seen in this study among Ca^{2+}-formed aGUVs, where their DiD intensity was more frequently above the expected value rather than below. This discrepancy could again be due to the differences in membrane composition or hemifusion conditions, though it is unclear what the reasoning for such causation would be. It is also uncertain why the relationship is seen in the first place, as the number of Mg^{2+}-formed aGUVs with higher than expected DiD intensity was similar to the number with lower than expected. It could be that Ca^{2+} is promoting the retention of DiD in the GUVs during hemifusion, though the mechanism behind this possible interaction is unclear.

In addition to compositional variability, the vesicles in this study also displayed variability with respect to size. For example, sGUVs were consistently larger than aGUVs, likely a result of the osmotic shrinking of sGUVs when adding the buffers to induce hemifusion (which could have slight osmolarity differences). Additionally, vesicles prepared in high salt buffer were consistently smaller than those made in low salt, which is presumably a result of the sGUV formation process yielding smaller vesicles with the high salt buffer procedure. There is likely nothing beyond the initial sGUVs being smaller that made the high salt buffer aGUVs smaller than those in low salt buffer. This idea is supported by the fact that the ratio of the average sGUV diameter to the average aGUV diameter was the same in both low and high salt buffer, indicating that sGUVs in both buffers decrease in size by the same factor when being converted into aGUVs. Though despite all these differences in vesicle size, it does not seem like the size of an aGUV influences whether it will have the desired composition or not, as there was no correlation between vesicle diameter and range-passing. It also does not seem like a vesicle's size has any influence on its fluorescence data, which is shown in Appendix A.

6. Conclusions

In conclusion, a new method for the fabrication of PS-containing aGUVs was derived based on research performed by Enoki et al (*14*). This method involves using Ca^{2+} or Mg^{2+} to induce hemifusion between the outer leaflets of sGUVs and an SLB containing PS, allowing the leaflets to exchange lipids. EDTA is then added to fission the membranes, freeing the GUVs, which should now have an unchanged inner leaflet composition, but an outer leaflet composition equal to that of the SLB. This hemifusion process occurs fast enough to be unperturbed by the tendency of PS to form domains in the presence of Ca^{2+}. Using fluorescence, it was shown this method yields aGUVs that are variable in composition, but still have the expected composition on average. To get around this variability, the aGUVs can be filtered based on their fluorescence data to isolate just those with the expected composition. Using this method, PS-containing aGUVs can be prepared, used in an experiment to study the interactions of PS lipids (e.g., its binding interactions with proteins, the registration of PS domains in asymmetric membranes), then later have their fluorescence data assessed to determine which vesicles in the experiment were of the desired composition.

References

1. Kay, J. G.; Fairn, G. D. Distribution, Dynamics and Functional Roles of Phosphatidylserine Within the Cell. Cell Communication and Signaling **2019**, 17 (1), 126. DOI: 10.1186/s12964-019-0438-z.
2. Zachowski, A. Phospholipids in Animal Eukaryotic Membranes: Transverse Asymmetry and Movement. Biochem J **1993**, 294 (1), 1-14. DOI: 10.1042/bj2940001.
3. Balasubramanian, K.; Mirnikjoo, B.; Schroit, A. J. Regulated Externalization of Phosphatidylserine at the Cell Surface: Implications for Apoptosis. Journal of Biological Chemistry **2007**, 282 (25), 18357-18364. DOI: 10.1074/jbc.M700202200.
4. Fadok, V. A.; Voelker, D. R.; Campbell, P. A.; Cohen, J. J.; Bratton, D. L.; Henson, P. M. Exposure of Phosphatidylserine on the Surface of Apoptotic Lymphocytes Triggers Specific Recognition and Removal by Macrophages. J Immunol **1992**, 148 (7), 2207-2216.
5. Conesa-Zamora, P.; Lopez-Andreo, M. J.; Gómez-Fernández, J. C.; Corbalán-García, S. Identification of the Phosphatidylserine Binding Site in the C2 Domain That is Important For PKC Alpha Activation and in vivo Cell Localization. Biochemistry **2001**, 40 (46), 13898-13905. DOI: 10.1021/bi011303o.
6. Feigenson, G. W. On the Nature of Calcium Ion Binding Between Phosphatidylserine Lamellae. Biochemistry **1986**, 25 (19), 5819-5825. DOI: 10.1021/bi00367a071.
7. Vernier, P. T.; Ziegler, M. J.; Dimova, R. Calcium Binding and Head Group Dipole Angle in Phosphatidylserine−Phosphatidylcholine Bilayers. Langmuir **2009**, 25 (2), 1020-1027. DOI: 10.1021/la8025057.
8. Haverstick, D. M.; Glaser, M. Visualization of Ca2+-Induced Phospholipid Domains. Proc Natl Acad Sci U S A **1987**, 84 (13), 4475-4479. DOI: 10.1073/pnas.84.13.4475.
9. Neumann, B. M.; Kenney, D.; Wen, Q.; Gericke, A. Microfluidic Device as a Facile in vitro Tool to Generate and Investigate Lipid Gradients. Chem Phys Lipids **2018**, 210, 109-121. DOI: 10.1016/j.chemphyslip.2017.10.007.
10. Guo, H.-Y.; Sun, H.-Y.; Deng, G.; Xu, J.; Wu, F.-G.; Yu, Z.-W. Fabrication of Asymmetric Phosphatidylserine-Containing Lipid Vesicles: A Study on the Effects of Size, Temperature, and Lipid Composition. Langmuir **2020**, 36 (42), 12684-12691. DOI: 10.1021/acs.langmuir.0c02273.
11. Pautot, S.; Frisken, B. J.; Weitz, D. A. Engineering Asymmetric Vesicles. Proc Natl Acad Sci U S A **2003**, 100 (19), 10718-10721. DOI: 10.1073/pnas.1931005100.
12. Cheng, H.-T.; Megha; London, E. Preparation and Properties of Asymmetric Vesicles That Mimic Cell Membranes. Journal of Biological Chemistry **2009**, 284 (10), 6079-6092. DOI: 10.1074/jbc.M806077200.

13. Marquardt, D.; Heberle, F. A.; Miti, T.; Eicher, B.; London, E.; Katsaras, J.; Pabst, G. 1H NMR Shows Slow Phospholipid Flip-Flop in Gel and Fluid Bilayers. Langmuir **2017**, 33 (15), 3731-3741. DOI: 10.1021/acs.langmuir.6b04485.
14. Enoki, T. A.; Feigenson, G. W. Asymmetric Bilayers by Hemifusion: Method and Leaflet Behaviors. Biophys J **2019**, 117 (6), 1037-1050. DOI: 10.1016/j.bpj.2019.07.054.
15. Singer, S. J.; Nicolson, G. L. The Fluid Mosaic Model of the Structure of Cell Membranes. Science **1972**, 175 (4023), 720-731.
16. Nicolson, G. L. Update of the 1972 Singer-Nicolson Fluid-Mosaic Model of Membrane Structure. *Discoveries (Craiova)* **2013**, *1* (1), e3. DOI: 10.15190/d.2013.3.
17. Watson, H. Biological Membranes. Essays Biochem **2015**, 59, 43-69. DOI: 10.1042/bse0590043.
18. Harayama, T.; Riezman, H. Understanding the Diversity of Membrane Lipid Composition. Nat Rev Mol Cell Biol **2018**, 19 (5), 281-296. DOI: 10.1038/nrm.2017.138.
19. Casares, D.; Escribá, P. V.; Rosselló, C. A. Membrane Lipid Composition: Effect on Membrane and Organelle Structure, Function and Compartmentalization and Therapeutic Avenues. Int J Mol Sci **2019**, 20 (9). DOI: 10.3390/ijms20092167.
20. van Meer, G.; Voelker, D. R.; Feigenson, G. W. Membrane Lipids: Where They are and How They Behave. Nature Reviews Molecular Cell Biology **2008**, 9 (2), 112-124. DOI: 10.1038/nrm2330.
21. Devaux, P. F.; Morris, R. Transmembrane Asymmetry and Lateral Domains in Biological Membranes. Traffic **2004**, 5 (4), 241-246. DOI: 10.1111/j.1600-0854.2004.0170.x.
22. Daleke, D. L.; Lyles, J. V. Identification and Purification of Aminophospholipid Flippases. Biochim Biophys Acta **2000**, 1486 (1), 108-127. DOI: 10.1016/s1388-1981(00)00052-4.
23. van Meer, G. Lipids of the Golgi Membrane. Trends in Cell Biology **1998**, 8 (1), 29-33. DOI: 10.1016/S0962-8924(97)01196-3.
24. Daleke, D. L. Phospholipid Flippases. Journal of Biological Chemistry **2007**, 282 (2), 821-825. DOI: 10.1074/jbc.R600035200.
25. Anglin, T. C.; Liu, J.; Conboy, J. C. Facile Lipid Flip-Flop in a Phospholipid Bilayer Induced by Gramicidin A Measured by Sum-Frequency Vibrational Spectroscopy. Biophys J **2007**, 92 (1), L01-03. DOI: 10.1529/biophysj.106.096057.
26. Steck, T. L.; Ye, J.; Lange, Y. Probing Red Cell Membrane Cholesterol Movement with Cyclodextrin. Biophys J **2002**, 83 (4), 2118-2125. DOI: 10.1016/s0006-3495(02)73972-6.
27. Simons, K.; Fuller, S. D. Cell Surface Polarity in Epithelia. Annu Rev Cell Biol **1985**, 1, 243-288. DOI: 10.1146/annurev.cb.01.110185.001331
28. Simons, K.; van Meer, G. Lipid Sorting in Epithelial Cells. Biochemistry **1988**, 27 (17), 6197-6202. DOI: 10.1021/bi00417a001.

29. Matter, K. Epithelial Polarity: Sorting Out the Sorters. Current Biology **2000**, 10 (1), R39-R42. DOI: 10.1016/S0960-9822(99)00256-0.

30. Simons, K.; Ikonen, E. Functional Rafts in Cell Membranes. Nature **1997**, 387 (6633), 569-572. DOI: 10.1038/42408.

31. Sezgin, E.; Levental, I.; Mayor, S.; Eggeling, C. The Mystery of Membrane Organization: Composition, Regulation and Roles of Lipid Rafts. Nature Reviews Molecular Cell Biology **2017**, 18 (6), 361-374. DOI: 10.1038/nrm.2017.16.

32. Levental, I.; Levental, K. R.; Heberle, F. A. Lipid Rafts: Controversies Resolved, Mysteries Remain. Trends Cell Biol **2020**, 30 (5), 341-353. DOI: 10.1016/j.tcb.2020.01.009.

33. Nickels, J. D.; Chatterjee, S.; Stanley, C. B.; Qian, S.; Cheng, X.; Myles, D. A. A.; Standaert, R. F.; Elkins, J. G.; Katsaras, J. The in vivo Structure of Biological Membranes and Evidence for Lipid Domains. PLOS Biology **2017**, 15 (5), e2002214. DOI: 10.1371/journal.pbio.2002214.

34. Slochower, D. R.; Wang, Y.-H.; Tourdot, R. W.; Radhakrishnan, R.; Janmey, P. A. Counterion-Mediated Pattern Formation in Membranes Containing Anionic Lipids. Advances in Colloid and Interface Science **2014**, 208, 177-188. DOI: 10.1016/j.cis.2014.01.016.

35. Garg, S.; Rühe, J.; Lüdtke, K.; Jordan, R.; Naumann, C. A. Domain Registration in Raft-Mimicking Lipid Mixtures Studied Using Polymer-Tethered Lipid Bilayers. Biophysical Journal **2007**, 92 (4), 1263-1270. DOI: 10.1529/biophysj.106.091082.

36. Sarmento, M. J.; Hof, M.; Šachl, R. Interleaflet Coupling of Lipid Nanodomains – Insights From in vitro Systems. Frontiers in Cell and Developmental Biology **2020**, 8, Review.

37. Moreno, M. J.; Teles Martins, P. A.; Bernardino, E. F.; Abel, B.; Ambudkar, S. V. Characterization of the Lipidome and Biophysical Properties of Membranes from High Five Insect Cells Expressing Mouse P-Glycoprotein. Biomolecules **2021**, 11 (3). DOI: 10.3390/biom11030426.

38. Leventis, P. A.; Grinstein, S. The Distribution and Function of Phosphatidylserine in Cellular Membranes. Annu Rev Biophys **2010**, 39, 407-427. DOI: 10.1146/annurev.biophys.093008.131234.

39. Bollen, I. C.; Higgins, J. A. Phospholipid Asymmetry in Rough- and Smooth-Endoplasmic-Reticulum Membranes of Untreated and Phenobarbital-Treated Rat lLiver. Biochem J **1980**, 189 (3), 475-480. DOI: 10.1042/bj1890475.

40. Mirnikjoo, B.; Balasubramanian, K.; Schroit, A. J. Suicidal Membrane Repair Regulates Phosphatidylserine Externalization During Apoptosis. J Biol Chem **2009**, 284 (34), 22512-22516. DOI: 10.1074/jbc.C109.022913.

41. Florine, K. I.; Feigenson, G. W. Influence of the Calcium-Induced Gel Phase on the Behavior of Small Molecules in Phosphatidylserine and Phosphatidylserine-Phosphatidylcholine Multilamellar Vesicles. Biochemistry **1987**, 26 (6), 1757-1768. DOI: 10.1021/bi00380a039.

42. Chan, Y. H.; Boxer, S. G. Model Membrane Systems and Their Applications. Curr Opin Chem Biol **2007**, 11 (6), 581-587. DOI: 10.1016/j.cbpa.2007.09.020.
43. Brian, A. A.; McConnell, H. M. Allogeneic Stimulation of Cytotoxic T Cells by Supported Planar Membranes. Proc Natl Acad Sci U S A **1984**, 81 (19), 6159-6163. DOI: 10.1073/pnas.81.19.6159.
44. Kresse, K. M.; Xu, M.; Pazzi, J.; García-Ojeda, M.; Subramaniam, A. B. Novel Application of Cellulose Paper As a Platform for the Macromolecular Self-Assembly of Biomimetic Giant Liposomes. ACS Applied Materials & Interfaces **2016**, 8 (47), 32102-32107. DOI: 10.1021/acsami.6b11960.
45. Pazzi, J.; Subramaniam, A. B. Nanoscale Curvature Promotes High Yield Spontaneous Formation of Cell-Mimetic Giant Vesicles on Nanocellulose Paper. ACS Applied Materials & Interfaces **2020**, 12 (50), 56549-56561. DOI: 10.1021/acsami.0c14485.
46. Rouser, G.; Fkeischer, S.; Yamamoto, A., Two Dimensional Thin Layer Chromatographic Separation of Polar Lipids and Determination of Phospholipids by Phosphorus Analysis of Spots. Lipids **1970**, 5 (5), 494-6 DOI: 10.1007/BF02531316.
47. Wen, Y.; Vogt, V. M.; Feigenson, G. W. Multivalent Cation-Bridged PI(4,5)P(2) Clusters Form at Very Low Concentrations. Biophys J **2018**, 114 (11), 2630-2639. DOI: 10.1016/j.bpj.2018.04.048.

Appendix A: Vesicle Curvature vs Fluorescence Intensity

When imaging vesicles to derive fluorescence intensities, a concern is that smaller vesicles could artificially yield higher intensities due to their higher degree of curvature. This situation is diagrammed in Figure A1A, which depicts a vesicle being imaged by the microscope. Imaging occurs along the z-axis, while the xy-plane is the plane of the stage. The vesicle (the black circle) is shown as a cross-section, which in full form, would extend along the y-axis to take a roughly spherical shape. The blue box on the vesicle bounds the area that is in focus during imaging, meaning that all parts of the vesicle within the box are what is chiefly seen by the microscope. Like the vesicle, this box would extend along the y-axis if shown in full. When the microscope takes an image, each point along the xy-plane is scanned individually for its fluorescence intensity. This intensity equals the sum of all fluorescence intensity at that (x,y) coordinate, and within the blue box. Therefore, if the box contains a greater amount of fluorophore molecules at an (x,y) coordinate, that point's intensity should be higher. For points that encompass the membrane of the vesicle, they could contain more fluorophore molecules on account of the membrane having a higher fraction of the fluorophore, or due to more of the membrane fitting within the box. This second situation causes more of the membrane, and thereby more of the fluorophore, to be at each (x,y) coordinate. This situation arises when the membrane is more curved (i.e., the vesicle is smaller), which results in more of it fitting within the box. Therefore, smaller vesicles could appear brighter due to simply having higher curvature, rather than actually having greater amounts of the fluorophore.

To determine the exact relationship between vesicle size and the amount of the vesicle's membrane able to be in focus at a time, an equation was derived for the arc length $\boldsymbol{s}$ shown in Figure A1A. This length is the distance along the vesicle's membrane from where it encounters the top of the box (**α**), to where it encounters the bottom (**β**). This arc length being larger means that more of the vesicle's membrane is in focus, as it represents the length of membrane in focus for one side of the vesicle's xz-plane cross-section. To derive its equation, the vesicle was first approximated as a perfect sphere, with the cross-section in Figure A1A being considered a perfect circle. Next, a vertical line was drawn down the center of the vesicle within the box. Two radius lines of length $\boldsymbol{r}$ were then drawn from the vesicle's center to points **α** and **β** to create two right triangles that intersect at the angle $\boldsymbol{\theta}$ and share the angle $\boldsymbol{\Phi}$. Next, the height of the box was defined as $\boldsymbol{h}$, and an equation was derived for $\boldsymbol{\theta}$ using the complementary angle theorem:

$$\boldsymbol{\theta} = \pi - 2 \cdot \arccos\left(\frac{0.5\boldsymbol{h}}{\boldsymbol{r}}\right) \tag{A1}$$

Using the arc length formula, this expression was used to derive the equation for $\boldsymbol{s}$:

$$\boldsymbol{s} = \boldsymbol{r}\left[\pi - 2 \cdot \arccos\left(\frac{0.5\boldsymbol{h}}{\boldsymbol{r}}\right)\right] \tag{A2}$$

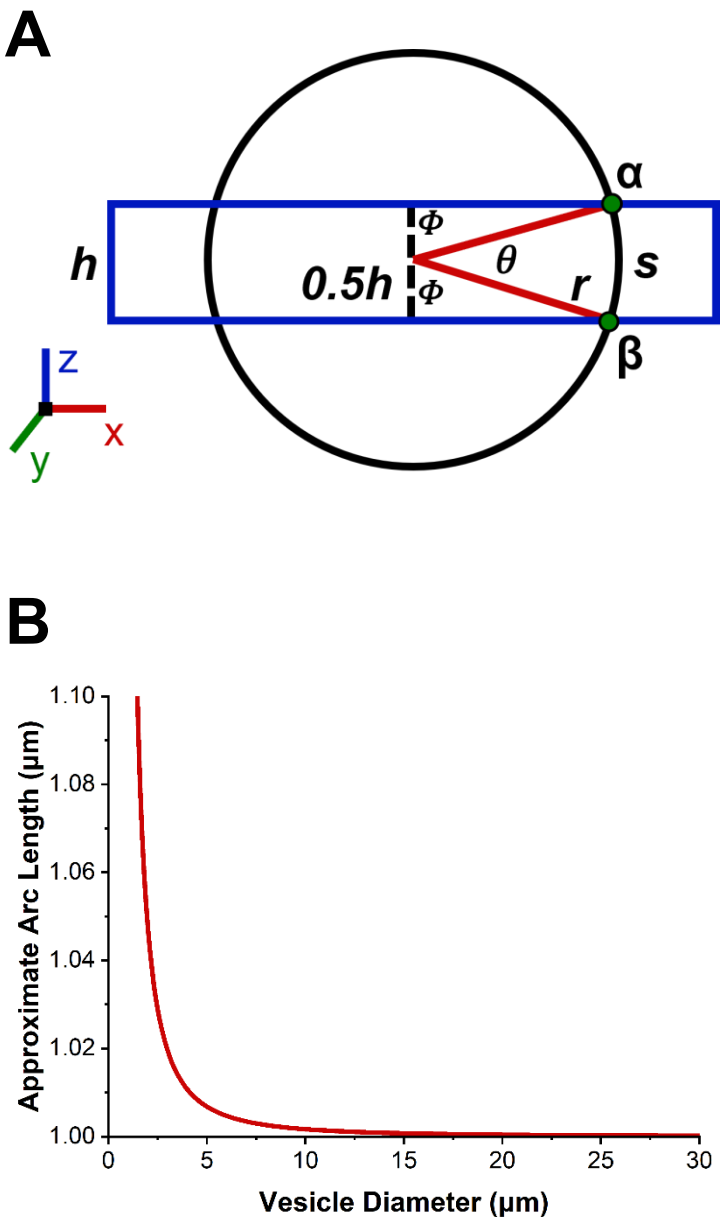

Figure A1. Relationship between vesicle diameter (curvature) and arc length in focus. (*A*) Diagram of a vesicle being imaged using the microscope. Imaging occurs along the z-axis, where the blue box is the area of the vesicle (the black circle) in focus. The "arc length in focus" is the distance labeled **s**. (*B*) Approximate arc length in focus (***s*** in panel A) vs vesicle diameter. The height of the area in focus (***h*** in panel A) is assumed to be 1 µm.

Using Equation A2, a plot of ***s*** vs vesicle size (diameter) was created, in which ***h*** was assumed to be 1 µm (which is the approximate value for the microscope used in this study). This graph is shown in Figure A1B. This plot demonstrates that for most vesicles, the value of ***s*** is effectively equal to ***h***, though it does start to increase as the vesicles get smaller than 7.5 µm in diameter.

However, the diameter must get below 2 µm before ***s*** increases to be even 10% higher than ***h***. Since in this study, all vesicles were above 2 µm, it seems the ***s*** of each could be considered equivalent. This relationship would mean that the amount of each vesicle's membrane in focus during imaging would effectively be equivalent, making the effects of vesicle curvature on intensity null.

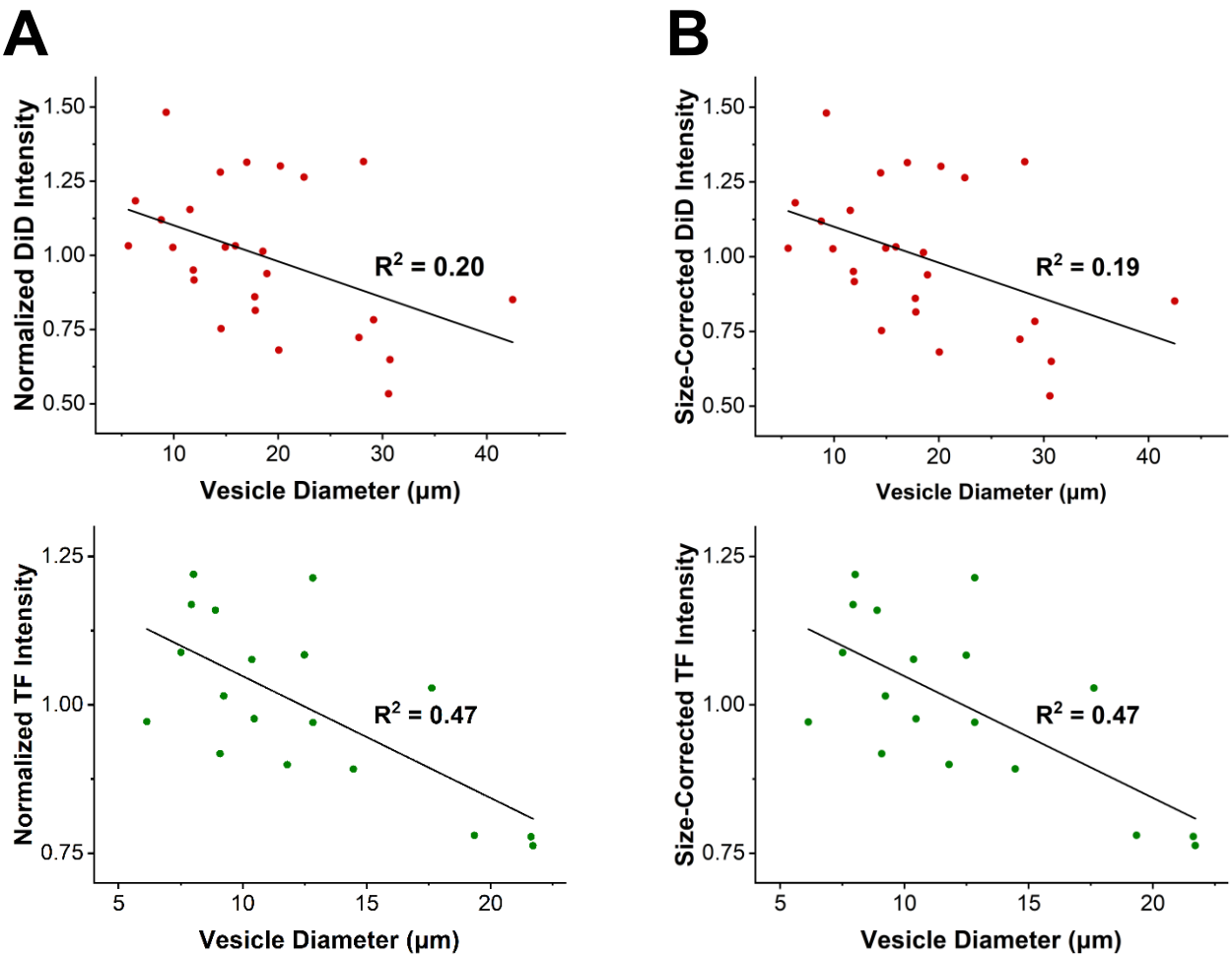

Figure A2. Relationship between sGUV diameter (curvature) and intensity in low salt buffer. (*A*) DiD or TF intensity vs vesicle diameter for DOPC/DiD (99.9/0.1 mol%) or DOPC/POPS/TF-PS (69.9/30/0.1 mol%) sGUVs respectively. All vesicles are in 180 mM glucose, 17 mM sucrose, 5 mM HEPES, pH = 7.4. Intensities are normalized by the average intensity of the corresponding sGUVs. The linear best fit line for each plot is shown in black. (*B*) Same as panel A, but each vesicle's intensity (before normalization) is divided by its approximate arc length in focus.

To more directly assess if vesicle curvature was influencing fluorescence intensity in this study, fit lines were constructed for the relationship between intensity and curvature (expressed as vesicle diameter) for various data sets of sGUVs. These fits are shown in Figure A2A. If curvature greatly

influences intensity, one would expect the fit lines to consistently overlap with the data and show a decreasing relationship between intensity and diameter. All lines showed this decreasing relationship, but all of them overlapped poorly with the data, having R^2 values less than 0.5. Therefore, it seems curvature has some effect on fluorescence intensity, but this effect is very small. To see if this possible effect can be lifted from the data, each intensity was normalized by the corresponding vesicle's ***s*** to try and remove any dependency on curvature. The fits were then redone, which is shown in Figure A2B. However, the fits were practically unchanged from how they looked before the normalization, and none of the intensity values changed by more than 1%. This result indicates that the slight decreasing relationship between intensity and curvature could be coincidental. Overall, based on all of these tests, it seems that any effects that curvature has on fluorescence intensity, at least in the context of this study, are negligible.